Phd. Thesis

Purely Magnetic Attitude Control Algorithm for Low Earth Orbit Satellites

Antonio Leopoldo Rodríguez Vázquez

UNIVERSIDAD DE SEVILLA
ESCUELA SUPERIOR DE INGENIEROS

DEPARTAMENTO DE INGENIERÍA ELECTRÓNICA

Author: Antonio Leopoldo Rodríguez Vázquez
Tutors: M. Ángeles Martín Prats
Franco Bernelli Zazzera

Dedicado a
Susana, Rafael y Lina.
Por todos estos años.

Abstract

In this work, a new method for magnetic satellite attitude control system design is presented. In this method, only magnetic actuators are needed and three axis pointing accuracy is achieved using a non linear technique called *Approximating Sequence of Riccati Equations (ASRE)*. This technique is based on transforming the nonlinear control problem into an equivalent time variant problem with the introduction of the iterative sequence corresponding to the system dynamics and another iterative sequence corresponding to the cost function to be minimized. The new problem can be solved as a sequence of two point boundary value problems using the costate transformation as a soft Constrained Problem.

The control system has been intensively proven for a wide variety of orbits and initial conditions. Model uncertainties and perturbations have been also taken into account. The results show that the control system works for a wide variety of orbits and that a better performance is achieved with high inclination orbits. Furthermore, the control strategy is able to control the satellite in case of large angular rates such as the ones that will remain after a detumbling phase using the well known Bdot algorithm for magnetic actuation.

Resumen

Este trabajo presenta una técnica de control de la orientación de un satélite utilizando únicamente actuadores de tipo magnético. El uso de este tipo de actuadores para el control de la orientación es conocido desde el lanzamiento de los primeros satélites. Sin embargo, debido a la naturaleza de la interacción magnética, el uso de este tipo de actuadores implica la falta en todo momento de un grado de libertad. Esto impide la aplicación de técnicas tradicionales de control, propiciando que tradicionalmente este tipo de actuadores hayan jugado un papel secundario en el sistema de control. No obstante, su bajo precio en comparación con otros actuadores y su facilidad en la operación y el mantenimiento han hecho que se utilicen en todo tipo de misiones.

En los últimos años, ha habido un gran avance teórico en las técnico de control no lineales. Aplicando una de estas técnicas llamada *Approximating Sequence of Ricatti Equations (ASRE)*, se consigue el control en 3 ejes. Esta técnica está basada en la transformación de un problema clásico de control no lineal en un problema equivalente en el tiempo donde se introducen una secuencia iterativa correspondiente a las ecuaciones dinámicas del sistema y otra secuencia iterativa que se corresponde a la función de coste que debe ser minimizada por el algoritmo de control. Este nuevo problema se resuelve como un problema del valor en los límites de dos puntos donde se utiliza el coestado para resolverlo. Además, se deja libre el punto final, lo que en la literatura se llama *Soft Constraint Problem* o problema con restricciones suaves.

El sistema de control se ha probado intensamente en una gran variedad de órbitas y condiciones iniciales. También se han realizado pruebas donde las perturbaciones y las incertidumbres posibles en el modelo se han tenido en cuenta. Los resultados demuestran que el sistema de control funciona de forma satisfactoria para una gran cantidad de órbitas, aunque los mejores resultados se consiguen en el caso de órbitas con alta inclinación. Además, el algoritmo de control es capaz de estabilizar la orientación del satélite en el caso de velocidades angulares grandes tales como las que podrían quedar después de una fase de desaceleración con un algoritmo de control bien conocido como es el Bdot.

Contents

List of Figures

List of Tables

1

Introduction

This thesis opens a new research line in the electronic engineering department of the university of Seville. The objective of this research work was to study the magnetic actuation of the satellites and the possibility to perform a three axis attitude control using only magnetorquers. The use of magnetorquers is well known in satellite attitude control as a secondary actuation method. However, in the past few year an interest in magnetic actuation has grown, because of the increasing number of small satellites to be launched. Small satellites are a very good platform for universities and research centers to test experimental payload and train engineers in space technology. Furthermore, the cost is reduced because the launch vehicle is usually shared with other small satellites or with a bigger satellite.

The thesis is divided in chapters. Each chapter can be read in-

dependently from each other. References are made when they are necessary, but depending on the background of the reader a review of some concept might not be necessary.

Chapter 2 describes the state of the art of the attitude control systems technology, with special focus on magnetic attitude control systems. Actuators for attitude control which are usually used together with magnetic actuators are also reviewed. Furthermore, other passive control techniques such as spin stabilization and gravity gradient are also briefly presented.

In chapter 3, the system model and the control algorithm are presented. Starting from the dynamic and kinematic equations of motion, the attitude equations are particularized for a nadir pointing spacecraft and are written in state dependent coefficient form. Finally, in section 3.5 the Approximating Sequence of Riccati Equations (ASRE) technique used to solve the control problem is introduced.

Simulations showing the performance and the methodology of the control system are presented in chapter 4. The main results of this work are described in this chapter. In chapter 5 the conclusions of the work are presented. The same conclusions are also presented in Spanish in chapter 6.

Every research work helps to understand or gives solution to a known [or unknown] problem. Furthermore, it opens new questions or topics which can be investigated in more detail. In chapter 7, the open topics which might be considered in the future are discussed.

2

Attitude Control Systems for Small LEO Satellites

In this section, a revision of the state of the art of the control techniques applied to satellites is reviewed. The survey is focused on Low Earth Orbit (LEO) satellites. First, the most common actuators for attitude control are presented in section 2.1. Then, passive control techniques are reviewed, with special focus on passive magnetic control techniques. Finally a deep review of active magnetic control techniques which involve the use of magnetorquers is presented.

2.1 Actuators for active attitude Control

Active attitude control is a subject of special interest in satellites. The environmental conditions in space require special types of actuators that are in use only in space applications. Magnetorquers are the best example of actuators that are only used in space. Other types of actuators like thrusters need to be designed specifically for space, although other uses in propulsion based on the same principle of operation are possible. In any case, a brief review of the most common actuators used for satellite attitude control is presented in this section. The advantages and disadvantages of each one are discussed. In the table 2.1, an overview of the properties of all the actuators is shown.

2.1.1 Magnetic Torquers

Magnetic Torquers are based on the Torque produced by a magnetic dipole with a certain magnetic moment. The torque produced by a magentic dipole with magnetic moment $\vec{m}$ in the presence of an static magnetic field $\vec{B}$ is:

$$\vec{T} = \vec{m} \wedge \vec{B} \tag{2.1}$$

The equation above has a physical and very intuitive meaning. Given a magnetic dipole in an external magnetic field, the dipole magnetic moment generates a force that tends to align itself with the external magnetic field. This effect has been used extensively in the past by the compass, where a magnetic needle attempts to align itself with the local direction of the Earth magnetic field.

The spacecraft itself might own a magnetic moment if it has ferromagnetic materials. This property can be used for passive magnetic control, as will be described in section 2.2.3. However, for actuation purposes, a controlled magnetic dipole can be generated. The easier way to generate a magnetic dipole is a current coil. The magnetic

Type	Advantages	Disadvantages
External type	Can control momentum build-up	
Thrusters	Insensitive to altitude Suit any orbit Can torque about any axis	Requires fuel On-off operation only Has minimum impulse Exhaust plume contaminants
Magnetic	No fuel required Torque Magnitude is controlable	No torque about the local field direction Torque is altitude and latitude sensitive Can cause magnetic interference
Gravity Gradient	No fuel or energy needed	No torque about the local vertical Low accuracy Low torque, altitude sensitive Libration mode needs damping
Internal types	No fuel required Can store momentum Torque magnitude is controllable	Cannot control momentum build-up
Reaction Wheels(RW) Momentum wheels (MW)	Continuous, accurate pointing capability Provide momentum bias	Non-linearity at zero speed
Control Moment Gyroscope (CMG)	Suitable for three axis control	Complicated mechanics and control

Table 2.1: Types of Torquers [1]

moment that can generate a current coil is:

$$\vec{m} = NIA\vec{n} \tag{2.2}$$

where N is the number of windings, I is the current intensity, A is the area enclosed by the coil and $\vec{n}$ is the unit vector that gives the direction of the moment. $\vec{n}$ is perpendicular to the area of the coil and its direction is given by the right hand rule of the direction of the current.

Torquers are usually designed to be implemented as rods. Therefore, a high number of windings is achieved, despite a small area. There is a wide range of sizes of magnetorquers available. The magnetic moment strength is a design parameter that has to suit the satellite mission.

The main advantages of magnetorquers are:

Low Power Consumption: Coils are usually made of a conductive wire of low electric resistance. Therefore, high currents can be achieved with small voltage drop minimizing the power dissipation. According to Ohm's law:

$$V = R \cdot I \tag{2.3}$$

Power consumption is $P = V \cdot I$, and substituting above equation:

$$P = I^2 \cdot R \tag{2.4}$$

Therefore, even for a large current, the small R keeps the power consumption small.

Simplicity and reliability: A coil has no moving parts, and the failure points are usually limited to the electrical connection with electronics control board. Furthermore, it needs no propellant making the operational time almost unlimited.

Simple operation: Magnetic coils can be operated as a full on - full off device or can be operated proportionally. This property makes them an excellent actuator for fine attitude control.

On the other hand, the main disadvantages are:

No torque along external magnetic field: From equation 2.1, it is straightforward to derive that a magnetorquer cannot produce any torque along the direction of the external magnetic field, which in satellites is usually the Earth magnetic field. This situation leads to the main inconvenience of magnetic actuation.

Difficult beyond LEO: Due to the dependence of the Earth magnetic field and provided that the magnetic field decays with the cube of the distance, maqnetorquers are almost useless beyond Low Earth Orbits.

2.1.2 Gyroscopic Actuators

Gyroscopic actuators are based on the mechanical properties of a wheel with a certain mass spinning at a certain speed. Their behavior can be modeled deriving each configuration from the Inertia moment conservation equation, this is:

$$\frac{d\vec{L}}{dt} = \frac{dI\vec{w}}{dt} = \sum \vec{N} \tag{2.5}$$

Depending on which part of the equation above is actuated, two different space actuators arise, Control Moment Gyroscopes or Momentum Exchange devices.

Control Moment Gyroscope

The Control Moment Gyroscope (CMG) has an angular momentum due to the rotor which is spinning about a spin axis with a constant angular rate. However, the spin axis is gimbaled. Therefore, a commanded gimbal rotation causes the direction of the angular momentum

vector to change. This turns into a torque which is perpendicular to both the spinning axis and the gimbal axis. The magnitude of this torque depends upon the speed of the rotor and the gimbal rotation rate.

First designs used a CMG just to aid another attitude control system, as for instance in [2], where a CMG is proposed to work together with a gravity gradient stabilization technique. An example of a full attitude control system design using CMGs can be found in [3].

In general, CMGs can be gimbaled about one axis or two, providing controllability around one or two axis. To provide full attitude control, at least 3 axis control capability is needed. However, usually more than three Single Axis CMGs are combined into a single platform and coordinated among them. Furthermore, a new generation of CMGs that combine both a CMG and a momentum wheel is available[4].

The main drawback of CMGs, even in array configuration, is the presence of kinematic singularities at certain gimbal configurations[5]. These singularities are points at which the array is incapable of instantaneously producing torque in a particular direction, which results in a loss of controllability. A major research topic over the last few years is the design of a control strategy that can handle those singularities constrained with algorithm calculation time and CMGs configurations[6].

Momentum and Reaction Wheels

Momentum and reaction wheels are usually called momentum exchange devices. These devices can be used for several purposes: to add stability against disturbance torques, to provide a variable momentum to allow operation at one revolution per orbit for Earth-oriented missions, to absorb cyclic torques, to transfer momentum to the satellite body for the execution of slewing maneuvers or for fine attitude control[7][1].

Reaction wheels have a nominally zero speed, and may be rotated in either direction in response to the control torques called by the

spacecraft control system. However it should be noted that at low or zero angular rate, the wheel displays a non-linear response due to *sticking friction*, which can impose an irregular motion on the spacecraft in this region. This problem is often circumvented by setting the nominal operating speed of the wheels above zero rate, at a few r.p.m. A typical example of precise pointing accuracy using reaction wheels is the Hubble Space Telescope Precision Pointing Control System[8].

Momentum wheels on the other hand have a high mean speed in order to provide momentum bias. The control torque will then slow down or increase the wheel speed. The momentum bias provides also gyroscopic stiffness to two axes, while the motor torque may be controlled to precisely point around the third axis[9].

For three axis control, three orthogonal reaction wheels will be the minimum requirement. One or more are normally added in an array configuration for redundancy purpose[10], in order to avoid a single-point failure. When more than one MW is used, the total bias is the vector sum of contributions from the separate wheels.

Both types of wheels provide momentum storage and need to be used in conjunction with other torquers for momentum unloading or momentum dumping when the internal momentum of the wheel reaches the saturation point. In [11] a momentum unloading technique for reaction wheels using magnetorquers is described.

2.1.3 Thrusters

Thrusters are based on expelling some mass out of the satellite at a certain velocity. This generates the thrust. Depending on the direction of the thrust generation, this propulsion method can be used for orbit insertion, station keeping and maneuvers or attitude control[9]. The propellant provides the mass to be ejected by the jet. The propellant is carried on board the satellite and is accelerated by the jet at the moment of providing the thrust.

The energy for the acceleration of the particles can be produced

by chemical reaction or thermodynamic expansion in case of Gas Jets. Gas Jets technology will be reviewed later in this section. When the energy is produced on board as electric power and is used to accelerate the particles electrodynamicly, then the thruster is called to be electric. The state of the art related to electric propulsion will be explained into detail later in this section.

Taking into account the Newton's Law of momentum conservation, the expelled propellant mass times its velocity is equal to the mass of the satellite times its change in velocity. Following this principle, the *Rocket Equation* is derived[12].

The thrust on the Spacecraft T is equal to the mass of the spacecraft M_s times its change in velocity v_s. On the other hand, the thrust given by the ejection of some propellant is the exhaust velocity of the propellant v_p times the time rate of change of the propellant mass m_p:

$$T = M_s \frac{dv_s}{dt} = -\frac{d}{dt}(m_p v_p) = -v_p \frac{dm_p}{dt} \tag{2.6}$$

The total mass of the Spacecraft is the delivered mass m_d plus the propellant mass:

$$M_s(t) = m_d + m_p \tag{2.7}$$

M_s changes due to the consumption of the propellant, so the time rate of change of the total mass is:

$$\frac{dM_s}{dt} = \frac{dm_p}{dt} \tag{2.8}$$

Substituting equation 2.8 into 2.6 results in

$$M_s \frac{dv_s}{dt} = -v_p \frac{dM_s}{dt} \tag{2.9}$$

which can be written as

$$dv_s = -v_p \frac{dM_s}{M_s} \tag{2.10}$$

Assuming a motion in a straight line, the equation above can be solved by integrating from the spacecraft initial velocity, v_i, to the final velocity, v_f, during which the mass changes from its initial value, $m_d + m_p$ to its final delivered mass, m_d:

$$\int_{v_i}^{v_f} dv = -v_p \int_{m_d+m_p}^{m_d} \frac{dM}{M} \tag{2.11}$$

and solving this equation gives:

$$\Delta v = v_p \; ln\left(\frac{m_d}{m_d + m_p}\right) \tag{2.12}$$

The *specific impulse* (I_{sp}), can be defined to be equal to the propellant exhaust velocity divided (v_p) by the gravitational acceleration g. The change in velocity of the spacecraft is then:

$$\Delta v = (I_{sp} \cdot g) \; ln\left(\frac{m_d}{m_d + m_p}\right) \tag{2.13}$$

Equation 2.13 shows that for a mission to reach a certain delta-v and a final delivered mass m_d, the propellant mass m_p can be reduced by increasing the I_{sp} of the propulsion system. Reducing the propellant mass of a spacecraft has obviously implications for the launch vehicle size and cost.

If equation 2.13 is solved for the propellant mass:

$$m_p = m_d \left[e^{\Delta v / I_{sp} \cdot g} - 1\right] \tag{2.14}$$

It is straightforward to say that the propellant mass increases exponentially with the delta-v required for a mission. Thrusters that provide a large propellant exhaust velocity compared to the mission Δv will have a propellant mass that is only a small fraction of the initial spacecraft wet mass.

A comparison among different thrusters technologies in terms of I_{sp} can be found in table 2.2[9]. Those technologies will be described briefly in the following subsections.

Thruster	I_{sp}	Input Power(kW)	Propellant
Cold Gas	50 - 75	–	Various
Monoprop	150 - 225	–	N_2H_4
Biprop	300 - 450	–	Various
Resistojet	300	0.5 - 1	N_2H_4
Arcjet	500 - 600	0.9 - 2.2	N_2H_4
Ion Thruster	2500 - 3600	0.4 - 4.3	Xenon
Hall Thrusters	1500 - 2000	1.5 - 4.5	Xenon
PPT	850 - 1200	<0.2	Teflon

Table 2.2: Thrusters comparison table

Gas Jets

Gas jets can be classified depending on the origin of the obtained energy. They are classified as hot gas when the energy is derived from a chemical reaction or cold gas when it is derived from the latent heat of a phase change, or from the work of compression if no phase change is involved[7]. In general, chemical jets can produce higher thrust and I_{sp} than cold gas jets. Cold gas jet propulsion is more consistent, specially in pulsed actuation systems where the chemical thruster needs the chemical reaction to arrive to a steady state.

Jets have big advantages over magnetic coils[1]. First, in distant orbits, coils are useless because the magnetic field of the Earth is too weak to perform a strong interaction with it, whereas thruster's torque is independent of the altitude. Second, control laws for jets are simpler than those for coils. Where the coils have a high dependent torque magnitude and direction on the available external magnetic field, gas jets thrusters can be arranged in a configuration such that the torque direction and magnitude is independent of the external environment.

The propellant supply required for jets is the major limitation on their use. A fuel budget is an important part of mission planning for any system using jets. Other considerations are the overall weight of the system[13] and the need to position thrusters where the exhaust

will not affect the spacecraft in case of corrosive propellants.

Although Control laws are easier to design where no external constraint on the available torque is considered, gas jets have another disadvantage for attitude control. Gas Jet Thrust Impulse cannot be fine regulated. In fact, although variable impulse or very finely regulated thrust jets are available or under research nowadays[14], the actuation should have traditionally been on or off. This has several drawbacks[15]. The fist one is the existence of limit cycles which affects the on-off operation[16]. Those limit cycles can be reduced when the impulse of the thruster is low enough. The second one is that jets have rise and fall time in the order of milliseconds[17]. Therefore, fine attitude control is only possible if a precise modeling of the thrust during rise and fall times so that thrusters performance during on and off is introduced and considered in the attitude control systems.

As described in chapter 17 of [9], thrusters are needed in most satellite missions for orbit insertion or station keeping. They can contribute to attitude control, but due to their high specific impulse and thrust they are not so adequate for fine attitude control. However, they have been used in many attitude control systems together with gyroscopic actuators (section 2.1.2) for momentum dumping[18] or with magnetic torquers[19] (section 2.1.1).

Electric Thrusters

Electric Propulsion is a technology which can generate thrust by accelerating charged particles and expelling them out of the spacecraft at high expulsion velocities[12]. Increasing the propellant exhaust velocity turns into a reduction of the mass propellant for a given amount of Thrust, as discussed in equation 2.14.

A working description of electric thrusters can be found in reference [20]. Here, a classification of Electric Thruster is given:

Resistojet: Resistojets are electrothermal devices in which the exhaust velocity of the propellant is due to thermal heating, which

is achieved by a resistively heated element.

ArcJect: Arjects are also electrothermal thrusters where the propellant is heated by means of a high current arc.

Ion Thrusters: Ion thrusters are based on plasma generation techniques to ionize the propellant. Then the ions are accelerated by creating a controlled high voltage electric field and expelled at very high exhaust velocities.

Hall Thrusters: This type of electrostatic thruster utilizes the Hall effect to generate the plasma. Hall thruster efficiency and specific impulse is somewhat less than that achievable in ion thrusters, but the thrust at a given power is higher and the device is much simpler and requires fewer power supplies to operate.

Pulsed Plasma Thrusters: A Pulsed Plasma Thruster (PPT) uses a pulsed electric discharge to generate the ionized plasma out of a solid propellant. Teflon is typically used as the propellant. The ions are then accelerated to high exhaust velocities. The pulse rate is used to determine the thrust level.

The possibility of electric propulsion started in the beginning of the 20th century with Robert H. Goddard and K. E. Tsiolkovsky. History of Electric propulsion is reviewed in [21] up to mid 40s.

Tsiolkovsky studied the rocket propulsion, and suggested the use of particles with small mass as propellant in 1911. He pointed out that the electrons moved in a cathode ray tube at velocities 10.000 times grater than that of the ordinary products of combustion flying from the reactive tubes.

By the same time, in 1906, Goddard thought about the possibility of liberating electrons at the speed of light using electric potential to accelerate them. In 1913, Goddard filed the first patent for producing *electrically charged particles*. Continuing with his research, Goddard filed in 1917 another patent that is the first documented *electrostatic*

on accelerator intended for propulsion. He also realized the potential of the invention because he achieved the greatest exhaust velocities produced so far, but those velocities could be increased by a higher electrical potential. With the beginning of World War I, Goddard devoted himself to chemical rocket launch vehicles.

Electric Propulsion started a hibernation era overwhelmed by chemical propulsion. The electrical potential and energy needed by electric thrusters were not easily achievable on board satellites during the following years.

In-depth research activities were carried on during 60s and 70s. In [22], the main advances in the technology and the first demonstrators on orbit up to 1969 are reviewed. Special mention deserves the Space Electric Rocket Test (SERT) program and the USAF electric propulsion flight tests called Program 661A[23].

Over the past 20 years, many programs have demonstrated the feasibility and the advantages of electric propulsion for every kind of satellites and applications, ranging from deep Space missions[24], trajectory optimization[25], geostationary telecommunication satellites where a failure of the launcher forced the thruster to unexpected mission accomplishments[26] or, what is more aligned with the topic of this work, the attitude control of microsatellites[27].

There is still an open field for innovation in ion thrusters. For instance in [28], a detailed description of the requirements for the next electric propulsion thruster under research is presented.

2.1.4 Non Conventional Actuators

There are several actuators which are under research or are not conventional because the technology is not mature enough or even just under theoretical research.

In [29], a broad review of propulsion in space under basic research is given. One example of these propulsion methods under research are the works presented by Brito[30] where an interaction between

dielectric media and electromagnetic field is described. In a more recent paper, the same author realizes that more research needs to be done[31].

Others known actuators are those based on fluid dynamics. The first reference on the use of fluids for satellite passive attitude damping is from [32]. In this patent, the author presents a fluid ring made of small diameter pipes surrounding the perimeter of satellite and claiming that the circulated fluid can induce control moments to stabilize the spacecraft. In [33], an improved system for accelerating the fluid mass through different fluid paths is presented.

In more recent works, the study of the satellite system including the fluid ring is overtaken[34]. In [35], a control system is presented with the integration of four fluid rings as main actuators.

Essentially, the fluid rings have the same principle of operation as a momentum wheel. The main advantage over the momentum wheel is that they can produce the same torque with a reduced mass, because the mass concentrates in the border of the ring, whereas the momentum wheel is usually solid. However, some disadvantages need to be addressed, such as the pumping method or the leakage and thermal protection.

2.2 Passive Control Techniques

The most common passive control techniques are spin stabilization, dual spin stabilization, gravity gradient and passive magnetic control[7].

2.2.1 Spin Stabilization

According to equation 2.5, if a satellite has an angular momentum vector $\vec{L}$, a torque $\vec{N}$ in the direction of $\vec{L}$ will increase or decrease the magnitude of $|L|$, but not its direction. On the other hand, if the torque is perpendicular to $\vec{L}$, only the direction of $\vec{L}$ will change, but

not its magnitude.

Spin stabilization has a lot of similarities with gyroscopic actuators. If the angular momentum L is large enough, a small torque will result in a small change in L. The basic requirement for spin stabilization is:

$$\left| \int \vec{N} dt \right| << \left| \vec{L} \right| \tag{2.15}$$

Equation 2.15 means that, in the case of cyclic perturbation torques, if the angular momentum of the satellite is large enough, the satellite will keep its attitude over the mission. On the other hand, if the perturbations are not cyclic, the time for which the passive control technique can be effective without an active one can be estimated.

Another variant of this control technique is the dual spin stabilized spacecraft. The technique is called dual spin because there are several parts of the satellite rotating at different speeds. Those parts can be the whole spacecraft and a momentum wheel or two parts of the body of the satellite. The dynamics of a spin stabilized spacecraft and dual spin stabilized spacecraft are in depth reviewed in [36].

2.2.2 Gravity Gradient

Every rigid object in the space which is not symmetrical is subject to a torque produced by the effect of the gravitational force over each point of the object. Assuming an spherical Earth, the gravitational force $d\vec{F}_i$ over an infinitesimal point i of mass dm_i is:

$$d\vec{F}_i = -\frac{\mu \vec{R}_i dm_i}{R_i^3} \tag{2.16}$$

where μ is the earth gravity constant, $\vec{R}_i$ is the vector Earth-to-satellite point and R_i is the module of $\vec{R}_i$. Therefore the torque produced by the Earth gravity is:

$$\vec{M}_g = \int_B \vec{r_i} \wedge d\vec{F}_i \tag{2.17}$$

where $\vec{r_i}$ is the vector between the center of gravity of the satellite and the point i within the satellite body.

Assuming that the center of mass of the satellite is the geometric center of the satellite which is also the origin of the body reference frame and $\vec{R_i} = \vec{R_s} + \vec{r_i}$, equation 2.17 can be approximated by[7]:

$$\vec{M_g} = \frac{3\mu}{R_s^3} \left[\vec{R_s} \wedge I \cdot \vec{R_s} \right] \tag{2.18}$$

where I is the inertia matrix. Several characteristics of the gravity gradient can be worked out of the equation above:

- Torque is orthogonal to the local vertical.
- Torque is inversely proportional to the cube of the distance to the center of the Earth.
- The torque vanishes for a spherical symmetric spacecraft.

A further study on the stability regions and motion of a passive gravity gradient attitude control system can be found in [36]. In brief, gravity gradient provides a passive self-aligning torque, but an oscillatory libration movement can occur if no damping is incorporated[37].

Damping methods can be passive[38] or active[39]. The most popular method for damping is active magnetic control, and will be reviewed later in section 2.3.2.

2.2.3 Magnetic

Attitude Control methods are a subject of interest since the Sputnik was launched in 1957. In fact, just after the launch of Sputnik I and II (launched about a month later), several researchers at John Hopkins Applied Physics Laboratory discovered that the doppler effect of the transmissions of the satellite could be measured on the Earth[40]. The first intention was to find out the orbit out of the doppler measurements. However, they quickly turn out to realize that they could do

the other way, this is, given a known orbit of the satellite, find out the position on the Earth out of the doppler measurements. The Transit program, which was the prelude for the GPS, was about to start.

The mission included a requirement of stability to stabilize the attitude of the spacecraft[41]. Any unknown velocity of the antenna would increase the uncertainty of the doppler shift. Furthermore, they were planning a long term mission, thus they need to gather some knowledge about the orientation of the solar panels with respect to the Sun. While precise pointing was not required, stability and simplicity were.

The solution to the attitude control was suggested by Robert E. Fishell. In [42], the attitude control systems of the first satellites of Transit are described. Passive attitude control is provided in these satellites by means of a fixed magnet rigidly mounted on the spacecraft. The satellites became orientated just in the same way as a compass points its needle.

They also realized the necessity of a method to remove the spinning energy of the spacecraft. The method utilized in those first spacecraft, were based on the use of highly permeable rods of specially prepared magnetic materials. This method depends on the fact that a permeable rod when spinning in the Earth's magnetic field will develop eddy current and hysteresis energy losses.

Although first proposed in 1963, this method of stabilization is still in use nowdays. In [43] and [44], a full description and design example of the permeable rods effect on the attitude is reviewed. In [45] or [46], another use of a passive magnetic attitude control system can be found. Finally, in [47], a full mathematical analysis of the magnetic hysteresis damper is presented.

2.3 Active Magnetic Control

Active magnetic control can be defined as the use of magnetorquers for attitude control of a satellite. As discussed in section 2.1.1, one of

the main drawbacks of magnetorques is the torque generation only in the plane perpendicular to the external magnetic field.

Despite this disadvantage, magnetorquers have been used in the space since the very beginning of the space era. Since the very first research works about active magnetic control[48], the absence of moving parts and no fuel consumption prevision have been identified as the main advantages of active magnetic control. Thus, active magnetic control has played several different roles in attitude control related tasks.

2.3.1 Magnetorquers and Momentum Bias

Probably the most used stabilization technique together with active magnetic control is momentum bias. Momentum bias stabilization has been discussed in section 2.2.1. The main advantage is the gyroscopic stiffness that this passive method gives to the spacecraft. However, a control strategy is needed to counteract the disturbing forces that can modify the spin. Active magnetic control is a very suitable control strategy to control the spin, specially together with another actuator such a momentum wheel. One of the first and very well explained works regarding 3 axis control on a spinning satellite is [49]. In this work, the authors present an active magnetic control system that, together with a flywheel that gives momentum bias, can perform the following functions:

1. Initial acquisition
2. Nutation damping
3. Precession Control
4. Momentum Bias Regulation

For the initial acquisition the B dot algorithm is used. This algorithm will be discussed later in 2.3.3. The momentum unloading

control law was proposed first in [48]. The momentum produced by the magnetorquers is set to:

$$\vec{m} = -K_u \vec{B} \wedge (\vec{H} - \vec{H_B}) \tag{2.19}$$

where $(\vec{H} - \vec{H_B})$ is the momentum to be unloaded. The torque produced can be derived merging equations (2.19) and (2.1):

$$\vec{T} = \vec{m} \wedge \vec{B} = -K_u \vec{B} \wedge (\vec{H} - \vec{H_B})\vec{B} = -K_u |B|^2 \Delta \vec{h}_\perp \tag{2.20}$$

where $\Delta \vec{h}_\perp$ is the momentum perpendicular to $\vec{B}$ which is to be unloaded. Of course no momentum in direction parallel to $\vec{B}$ can be unloaded. However, as the magnetic field in spacecraft body axis changes in direction along certain orbits, all the directions can be reached. Therefore, the total momentum can be controlled.

Nutation damping and precession control are achieved by means of a proportional control, where the value of the coefficients are bounded for stability purposes.The rejection capability to torques is very dependent on these gains and the total momentum of the spacecraft.

Many other strategies followed this work. In [50], an observer and a servo compensator approach is presented for roll/yaw control. Another control law based on the properties of periodic systems is discussed in [51]. In this work, the author compares his results with the work in [49], stating that a smaller momentum bias and better accuracy can be achieved by a periodic linear quadratic Gaussian control law.

Several modifications of the technique in [49] have been proposed for different uses. In [52] and [53] active attitude control systems for Sun pointing momentum biased satellites are designed. In [54] the same control system is applied to a small university satellite. In [55],the problem of optimal reaction wheel desaturation maneuver of a satellite using internal magnetorquers is discussed.

In [56] another set of algorithms for spin stabilized spacecraft are proposed for three mission stages:

1. Nutation damping. One coil is used, located on the satellite's symmetry axis and realizing Bdot algorithm.

2. Spin-up of the satellite about its symmetry axis to the necessary angular velocity. Two coils located in the equatorial plane of the satellite are used. It is assumed that the initial equatorial component of the angular velocity is small at this stage as a result of action of the algorithm of nutation dumping.

3. Reorienting the satellite's symmetry axis into a preset position in the inertial space. At this stage the discrepancy between the current angular momentum vector directed along the symmetry axis and the required direction in the inertial space decreases

In a more recent work [57][58], a spin stabilization control law by the use of magnetic only actuation is presented. It is shown that, with adequate orbit inclination, the control law globally asymptotically stabilizes a three inertial spacecraft, leading it to a desired spin condition in the inertial frame.

2.3.2 Magnetorquers and Gravity Gradient Boom

Gravity gradient passive stabilization has been discussed previously in section 2.2.2. In [59], a detailed design report of a satellite mission using gravity gradient and magnetorquers is presented. In this work, the authors analyze the control laws for all the operational phases of the mission, which are:

1. Detumbling

2. Spin Rate Control

3. Boom extension maneuver

4. Libration Damping, yaw control and stabilization

The pointing stabilization achieved by this technique is about 1 degree in all axis.

In [39], a less mathematical analysis of the benefits of active magnetic control use together with gravity gradient passive technique is shown.

Several designs for other satellites and new types of controllers followed this work. In [60] a gravity gradient design including active magnetic control for a small satellite is reviewed.

In [61], a comparison of the attitude control system described in [59] and other control algorithms is presented. Those algorithms are based on fuzzy logic and Linear Quadratic Regulation. All of the controllers were able to keep the pointing accuracy of the satellite to within 1 degree, although the best accuracy is achieved with fuzzy controller and the controller in [59].

Finally in [62], an state feedback PD control law for the magnetic attitude stabilization of a nadir pointing spacecraft is proposed. In presence of gravity gradient, the control law is proven to guarantee stability for obit inclinations grater than 0 degrees.

2.3.3 Active Magnetic Detumbling

In its simplest form, the detumbling mode control requires only the measurements of the magnetometer, and is based on a negative feedback of the derivative of the measured magnetic field vector[49]. This is the well known B-dot algorithm. The control torque and the actuator dipole moments are given by

$$\vec{m} = -K_B \dot{\vec{B}}_{pi} \quad ; \quad \vec{T} = \frac{B_{pi} \vec{\wedge} \vec{m}}{|B_p i|^2} \tag{2.21}$$

This simple feedback control has good performances when the angular velocity is large, since in this case it can be shown that the rate of change of the measured magnetic field vector depends primarily on the rate of change of the attitude of the satellite, therefore the rate of

change of the rotational kinetic energy is guaranteed to be negative.

$$\dot{\vec{B}_{pi}} = \dot{A}\vec{B_{orb}} + A\dot{\vec{B}_{orb}} \approx \dot{A}\vec{B_{orb}} \quad ; \quad \dot{E}_k \approx \vec{\omega}^T\vec{m} = -k_B \ \dot{\vec{B}}_{pi}^T\dot{\vec{B}_{pi}} \quad (2.22)$$

As the angular velocity becomes smaller, approximately less that half the orbit angular velocity, the intrinsic variations of the magnetic field along the orbit become more important, therefore the control can not guarantee energy dissipation under this assumption. This control law has been proved to release the angular momentum of the satellite exponentially, although in practice, due to saturation of the magnetorquers, the momentum decays linearly[63]. A more detailed study of the behavior of the b-dot algorithm can be found in [64].

In a more recent paper[65], the authors present an alternative version of the b-dot control law that guarantee global stability for active magnetic detumbling in presence of a time-varying magnetic field. This is achieved by defining the feedback gain such that it prevents the angular velocity vector from becoming parallel to the Earth magnetic field. Consequently the available control torque does not drop close to zero and a faster detumbling is obtained.

2.3.4 3-axis Magnetic Control

All the techniques presented so far are based on an inherent stability of the satellite's attitude. The stability can be because of gyroscopic stiffness (momentum biased satellites) or due to the design of the moment of inertia of the satellite (gravity boom). However, a bigger problem arises when the satellite has no mechanical nor physical stability.

This case is the main study of this work and has also been the subject of several works over the last few years. In [66], a good review of these techniques is available up to 2003. In this work, the authors classify the control techniques under three categories:

- Linear design methods

- Non-Linear design methods
- Predictive control

The main difference between these methods is the linearization of the attitude kinematics and dynamics of the attitude equations of a rigid solid in orbit in space. Despite the presentation of the equations of motion, all the techniques presented so far can be also classified depending on the design assumption made for problem statement. Therefore, the following classification is suggested:

- Periodic controllers
- Projection based controllers
- Full non-linear model controllers

Periodic Controllers

Periodic controllers are based on the periodic approximation of the magnetic field of the Earth as seen from the orbit of the spacecraft. The characteristics of the magnetic field will be reviewed later in section 3.3. This is a first order approximation and is quite good for high altitude orbit >5000Km.

Assuming the periodic nature of the magnetic field, the problem can be transformed into a periodic linear problem which can be stabilized by state periodic feedback or the more classical output feedback. A very good discussion and design of periodic controller and periodic control theory is presented in [67]. In this work, the author presents a wide range of controllers, form constant gain linear periodic controller to energy approaches for attitude control. Other works by the same author describes a finite horizon controller [68] and the design of H_2-optimal periodic controller[69]. Others designs of optimal linear periodic controllers are presented in [70][71][72][62][73].

The main advantage of periodic linear controllers is the use of Floquet's theory to prove stability[67][74]. Floquet stability analysis

computes the closed-loop state transition matrix for one period of the system and verifies that all of its eigenvalues have a complex magnitude less than unity.

Projection Based Controllers

Projection based controllers are based on the idea previously discussed in equations 2.19 and 2.20, and presented in [48].

The idea behind these techniques is fairly simple. The main drawback of active magnetic control is the lack of one degree of freedom for 3 axis torque generation. In fact, torque can only be produced in the plane orthogonal to the local direction of the magnetic field ($\vec{B}$). Therefore a possible design rule is, given the ideal torque (T_{ideal}) for a fully actuated spacecraft, project that torque over the orthogonal plane of $\vec{B}$ obtaining the effective magnetic torque (T_{mag}). The moment generated by this technique and the torque applied are given by equations 2.23 and 2.24, where $S(\vec{B})$ is the skew-symmetric matrix of vector $\vec{B}$.

$$\vec{m} = \frac{1}{|\vec{B}|^2} S(\vec{B})' \vec{T_{ideal}} \tag{2.23}$$

$$\vec{T_{mag}} = S(\vec{B})\vec{m} = \frac{1}{|\vec{B}|^2} S(\vec{B}) S(\vec{B})' \vec{T_{ideal}} \tag{2.24}$$

Examples of projection based controller can be found in the aforementioned [48] or [49]. In [66] a predictive controller which uses this technique is also suggested for attitude control. In a more recent work[75], the MATLAB toolbox for periodic system is used to design discrete controllers based on both optimal periodic controller and averaging techniques controller.

Non-linear controllers

Perhaps the most popular non linear controller proposed for attitude control is the B-dot detumbling algorithm which has been discussed

previously in section 2.3.3. In [76], a related line of work has been devoted to the nonlinear analysis of a magnetic scheme based on the sole measurement of the magnetic field vector $\vec{B}$

Other nonlinear control system is presented in [77]. In this work, the authors implement and compare six different algorithms for attitude control for nutation damping, coarse reorientation, spinning and fine reorientation of the satellite.

3

Attitude Control Systems Design

Satellite attitude control systems have been reviewed in the previous chapter. In this chapter the equations that will be used in the model of the system are derived. First, reference frames are defined in section 3.1. Then the dynamics and kinematics equation of motion are described in section 3.2. After that, a description of the magnetic field

of the Earth model is presented in section 3.3 and is included in the system model as it is described in section 3.4. Finally, the control technique used to stabilize the attitude is presented in section 3.5.

3.1 Reference Systems

There are several coordinate systems that will be used through the thesis. They are represented in figure 3.1. These coordinate systems are:

- **Body Coordinate System** (pi): This coordinate reference system is associated to the satellite body. It is centered in the center of mass of the satellite and its axis are oriented along the principal axis of the satellite. It is assumed that the principal axis of the satellite are the same as the *geometrical* axis.
- **Local Vertical Local Horizontal** (LVLH): This coordinate system is centered in the center of mass of the satellite. The y axis points toward the center of the earth (nadir), the p axis is perpendicular to the orbital plane in the direction of the angular velocity and the r axis is perpendicular to both p and y resulting in the tangential direction to the the orbit and in the sense of the instantaneous velocity.
- **Orbit Perifocal** (orb): The orbit perifocal coordinate system is a system for which the plane of the spacecraft orbit is the equatorial plane of the coordinate system. It is centered in the center of the Earth. The e axis is parallel to the line from the center of the Earth to the Ascending Node (AN) of the spacecraft orbit, the h axis is parallel to the orbit normal and the p axis can be found using the right hand rule.
- **Earth Centered Earth Fixed** (ECEF): This coordinate system is fixed to the Earth. Its 3 axis is aligned with the rotation axis of the Earth, the 1 axis point towards the intersection of

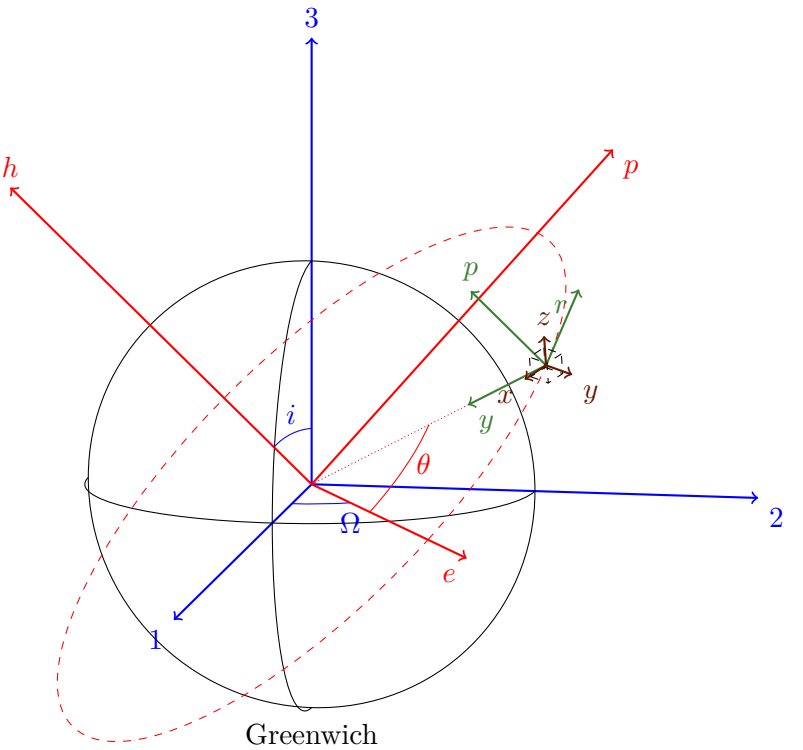

Earth

Earth Centered Earth Fixed (ECEF) Frame

Orbit Perifocal (orb) Frame

Local Vertical Local Horizontal (LVLH) Frame

Principal Inertia (PI) Body Frame

where Ω is the Right Ascension of the Ascending Node (RAAN), i is the orbit inclination and θ is the satellite anomaly.

Figure 3.1: Reference Systems

the Greenwich meridian with the Equator and the 2 axis is perpendicular to both 3 and 1 and completes the right hand rule.

Further clarification about the calculation and transformation between different axis can be found in appendix B.

3.2 Attitude Equations of Motion

In this section, the derivation of the dynamics and kinematics equations is described. Additional information on satellite mechanics can be found in [7].

3.2.1 Torque-Free Motion of a Rigid Body

First of all, we define the angular momentum $\vec{L}$ of a point mass m at a position $\vec{r}$ relative to some arbitrary origin as

$$\vec{L} = \vec{r} \wedge \vec{p} = \vec{r} \wedge m\vec{v} \tag{3.1}$$

where $\vec{p}$ is the momentum and $\vec{v}$ is the velocity of the point. For n points:

$$\vec{L} = \sum_{i=1}^{n} \vec{L_i} = \sum_{i=1}^{n} \vec{r} \wedge \vec{p_i} \tag{3.2}$$

The principle of angular momentum conservation settle that the angular momentum $\vec{L}$ remain fixed in an inertial coordinate reference system if there are no external torques. Therefore, the angle between the angular momentum $\vec{L}$ and the angular velocity of the rigid body $\vec{\omega}$ depends on the initial velocity and mass distribution. This let us to define a set of axis which are called th **principal axes** such that, for a rotation about a principal axis $\vec{P}$, $\vec{L}$ is parallel to $\vec{\omega}$, or:

$$\vec{L} = I_p\vec{\omega} = I_p\omega\vec{P} \tag{3.3}$$

where I_p is a constant of proportionality called *principal moment of inertia* which, for a collection of point masses,

$$I_p = \sum_{i=1}^{n} m_i r_i^2 \tag{3.4}$$

Regarding the parallelism among the angular momentum $\vec{L}$, the angular velocity vector $\vec{\omega}$, the principal axis $\vec{P}$ and the geometrical axis $\vec{z}$, there are three different movements:

- **Rotation**: $\vec{z} \| \vec{L} \| \vec{\omega} \| \vec{P}$
- **Coning**: $\vec{z} \nparallel \vec{L} \| \vec{\omega} \| \vec{P}$
- **Nutation**: $\vec{L} \nparallel \vec{\omega} \nparallel \vec{P}$
  - $\vec{P}$ and $\vec{\omega}$ rotate about $\vec{L}$
  - $\vec{P}$ is fixed in the pi reference frame.
  - $\vec{\omega}$ rotates in the pi reference frame and in the inertial reference frame.
  - $\vec{L}$ is fixed in the inertial frame but rotates in the pi reference frame.

3.2.2 Response to Torques

The section above deals with the torque-free motion of a S/C. Now we want to analyze what happens when we apply some forces to the S/C. Differentiation with respect to time of the eq. 3.2 above gives:

$$\begin{aligned} \frac{d}{dt}\vec{L} &= \sum_{i=1}^{n} \frac{d}{dt}\vec{L_i} = \sum_{i=1}^{n} \frac{\delta}{\delta t}\vec{r_i} \wedge m_i\vec{v_i} = \\ &= \sum_{i=1}^{n} \vec{v_i} \wedge m_i\vec{v_i} + \vec{r_i} \wedge m_i\vec{a_i} = \sum_{i=1}^{n} \vec{r_i} \wedge \vec{F_i} = \\ &= \sum_{i=1}^{n} \vec{N_i} \equiv \vec{N} \end{aligned} \tag{3.5}$$

So the angular momentum can be changed only if some torque is applied to the S/C. Notice that this equation can only be used in an inertial reference frame. Depending on the direction of the torque applied with respect to the angular momentum, the effects are different:

- If $\vec{N} \parallel \vec{L} \Rightarrow \left|\vec{L}\right| \uparrow$ or $\left|\vec{L}\right| \downarrow$
- If $\vec{N} \nparallel \vec{L} \Rightarrow \angle\vec{L} \uparrow$ or $\angle\vec{L} \downarrow$

The change of direction of $\vec{L}$ due to $\vec{N}$ is called *precession*. If $\left|\vec{N}\right| \ll \left|\vec{L}\right|$, then it is called drift.

3.2.3 Kinematic Equations of Motion

Quaternions

There are several representations for the attitude. One of the most used in space is the quaternion representation. The quaternion representation is usually used to indicate the rotation about one axis of a reference frame with respect to another. In the S/C case, it is used to represent the rotation of the Body Coordinate Reference System with respect to the Control Coordinate Reference System. Thus the quaternion itself gives an orientation in the space.

Let $\vec{q}(t)$ represent the orientation of the S/C at time t; $\vec{q}(t + \Delta t)$ represents the orientation at time $t + \Delta t$ and $\vec{q'}(t + \Delta t)$ represents the orientation at time $t + \Delta t$ relative to the position at time t; then:

$$\vec{q'} = \begin{bmatrix} q'_1 \\ q'_2 \\ q'_3 \\ q'_4 \end{bmatrix} = \begin{bmatrix} e_u \sin\left(\frac{\Delta\phi}{2}\right) \\ e_v \sin\left(\frac{\Delta\phi}{2}\right) \\ e_w \sin\left(\frac{\Delta\phi}{2}\right) \\ \cos\left(\frac{\Delta\phi}{2}\right) \end{bmatrix} \tag{3.6}$$

where e_u, e_v and e_w are the components of the rotation axis unit vector along the $\vec{u}$, $\vec{v}$ and $\vec{w}$ triad at time t. The following small angle approximations apply:

$$\cos\left(\frac{\Delta\phi}{2}\right) \approx 1 \tag{3.7}$$

$$\sin\left(\frac{\Delta\phi}{2}\right) \approx \frac{1}{2}\omega\Delta t \tag{3.8}$$

$$\vec{q}(t+\Delta t) \approx \left[I + \frac{1}{2}\Omega\Delta t\right] \cdot \vec{q}(t) \tag{3.9}$$

where Ω is the skew-symmetric matrix of the angular velocity:

$$\Omega = \begin{bmatrix} 0 & \omega_w & -\omega_v & \omega_u \\ -\omega_w & 0 & \omega_u & -\omega_v \\ \omega_v & \omega_u & 0 & \omega_w \\ -\omega_u & -\omega_v & -\omega_w & 0 \end{bmatrix} \tag{3.10}$$

If we make the Δt differential, we have the kinematic equation of motion:

$$\boxed{\frac{\delta\vec{q}}{\delta t} = \frac{1}{2}\Omega\vec{q}} \tag{3.11}$$

Euler Angles

Another representation of the kinematics equations are the Euler angles. The Euler angles represent kinematics by means of a sequence of simple rotations. Although there is no unique sequence for forming the Euler angles, there are widely accepted sets for specific applications. In this case, the 2-1-3 sequence will be used. Let ϕ represent the angle about the y-axis, θ about the x-axis and ψ around the z-axis.

Therefore, the angular rotation of one reference system about another can be described through the transformation matrix of equation 3.12.

$$C_n^b = C_{z''}(\psi)C_{x'}(\phi)C_y(\theta) \tag{3.12}$$

y-axis: the direction cosine matrix that rotates an angle ϕ about $\vec{u} = [0\ 1\ 0]$ is:

$$C_y(\phi) = \begin{bmatrix} \cos(\phi) & 0 & -\sin(\phi) \\ 0 & 1 & 0 \\ \sin(\phi) & 0 & \cos(\phi) \end{bmatrix} \tag{3.13}$$

x-axis: the direction cosine matrix that rotates an angle θ about $\vec{u} = [1\ 0\ 0]$ is:

$$C_x(\theta) = \begin{bmatrix} 1 & 0 & 0 \\ 0 & \cos(\theta) & \sin(\theta) \\ 0 & -\sin(\theta) & \cos(\theta) \end{bmatrix} \tag{3.14}$$

z-axis: the direction cosine matrix that rotates an angle ψ about $\vec{u} = [0\ 0\ 1]$ is:

$$C_z(\psi) = \begin{bmatrix} \cos(\psi) & \sin(\psi) & 0 \\ -\sin(\psi) & \cos(\psi) & 0 \\ 0 & 0 & 1 \end{bmatrix} \tag{3.15}$$

The Euler angles derivatives are obtained as functions of the body angular rate with respect to some reference frame as follows. We first observe that the Euler angles, and consequently their derivatives, are defined in different frames. If we reference all of them to the body frame, we get:

$$\vec{\omega_{pi}} = C_{z''}(\psi) \begin{bmatrix} 0 \\ 0 \\ \dot{\psi} \end{bmatrix} + C_{z''}(\psi) C_{x'}(\theta) \begin{bmatrix} \dot{\theta} \\ 0 \\ 0 \end{bmatrix} + C_{z''}(\psi) C_{x'}(\theta) C_y(\phi) \begin{bmatrix} 0 \\ \dot{\phi} \\ 0 \end{bmatrix} \tag{3.16}$$

Therefore:

$$\vec{\omega_{pi}} = \begin{bmatrix} \omega_x \\ \omega_y \\ \omega_z \end{bmatrix} = \begin{bmatrix} \dot{\theta}\cos(\psi) + \dot{\phi}\sin(\psi)\cos(\theta) \\ \dot{\phi}\cos(\psi)\cos(\theta) - \dot{\theta}\sin(\psi) \\ \dot{\psi} - \dot{\phi}\sin(\theta) \end{bmatrix} \tag{3.17}$$

Then, resolving for $\dot{\phi}$, $\dot{\theta}$, and $\dot{\psi}$, the kinematic equation expressed in Euler angles is derived:

$$\boxed{\begin{bmatrix} \dot{\phi} \\ \dot{\theta} \\ \dot{\psi} \end{bmatrix} = \begin{bmatrix} \frac{\omega_y \cos(\psi) + \omega_x \sin(\psi)}{\cos(\theta)} \\ \omega_x \cos(\psi) - \omega_y \sin(\psi) \\ \omega_z + (\omega_y \cos(\psi) + \omega_x \sin(psi)) \frac{\sin(\theta)}{\cos(\theta)} \end{bmatrix}} \tag{3.18}$$

3.2.4 Rate of Change of Vectors in Rotating Frames

Let $\vec{a}$ be a vector in the reference frame B and $\vec{a}^I$ the same vector in the inertial reference frame I. Let C^{BI} be the transformation matrix between the two reference frames. Thus,

$$\vec{a} = C^{BI}\vec{a}^I$$

Therefore, the product rule for differentiation gives

$$\frac{\delta \vec{a}}{\delta t} = \frac{\delta C^{BI}}{\delta t}\vec{a}^I + C^{BI}\frac{\delta \vec{a}^I}{\delta t}$$

The first term can be written as follows:

$$\frac{\delta C^{BI}}{\delta t}\vec{a}^I = \Omega^{BI}C^{BI}\vec{a}^I = \Omega^{BI}\vec{a} = -\omega^{BI} \wedge \vec{a}$$

where Ω^{BI} is the skew-symmetric matrix of ω^{BI}

The second term consists of the components in frame B of the vector $\frac{\delta \vec{a}^I}{\delta t}$, where the time derivatives are evaluated in the frame I. If we denote this vector by $\left(\frac{\delta \vec{a}^I}{\delta t}\right)_B$, the following equation is obtained

$$\frac{\delta \vec{a}}{\delta t} = -\omega^{BI} \wedge \vec{a} + \left(\frac{\delta \vec{a}^I}{\delta t}\right)_B \tag{3.19}$$

3.2.5 Angular Momemtum and Moment of Inertia Tensor

In equation 3.2 we introduced the angular momentum for N points. Let's suppose now that we define $\vec{r}_i$ as the sum of two vectors, one fixed for all the points and the other which is different for each point:

$$\vec{r}_i = \vec{R} + \vec{\rho}_i \tag{3.20}$$

Therefore, we can define $\vec{v}_i$ as the sum of two vectors:

$$\vec{v}_i = \vec{V} + \frac{\delta\vec{\rho}_i}{\delta t} \tag{3.21}$$

Substituting eqs. 3.20 and 3.21 in 3.2 yields

$$\begin{aligned} \vec{L} &= M\vec{R} \wedge \vec{V} + \vec{R} \wedge \frac{d}{dt}\left[\sum_{i=1}^{n} m_i\rho_i\right] \\ &\quad + \left[\sum_{i=1}^{n} m_i\rho_i\right] \wedge \vec{V} + \sum_{i=1}^{n} m_i\rho_i \wedge \frac{\delta\vec{\rho}_i}{\delta t} \end{aligned} \tag{3.22}$$

If we choose $\vec{R}$ coincident with the center of mass of the rigid body, this is, $\sum_{i=1}^{n} m_i\vec{\rho}_i = 0$, we simplify the equation to

$$\vec{L} = \sum_{i=1}^{n} m_i\rho_i \wedge \frac{\delta\vec{\rho}_i}{\delta t} \tag{3.23}$$

The components of $\vec{\rho}_i$ in the spacecraft frame are constant, but the components of $\frac{\delta\vec{\rho}_i}{\delta t}$ are not zero if the spacecraft is rotating with an instantaneous angular velocity ω, because the vector $\frac{\delta\vec{\rho}_i}{\delta t}$ is the rate of change of $\vec{\rho}_i$ *relative to inertial coordinates, resolved along S/C axes.* Therefore, using eq.3.19, we have

$$\frac{\delta\vec{\rho}_i}{\delta t} = -\omega \wedge \vec{\rho}_i + \left(\frac{\delta\vec{\rho}_i}{\delta t}\right)_{Body} \Rightarrow \left(\frac{\delta\vec{\rho}_i}{\delta t}\right)_{Body} = \omega \wedge \vec{\rho}_i \tag{3.24}$$

Substituting eq 3.24 into eq 3.23 we have:

$$\vec{L} = \sum_{i=1}^{n} m_i \vec{\rho}_i \wedge (\vec{\omega} \wedge \vec{\rho}_i) = \sum_{i=1}^{n} m_i \left[\vec{\rho}_i^{\,2} \vec{\omega} - (\vec{\rho}_i \cdot \vec{\omega}) \, \vec{\rho}_i \right] \tag{3.25}$$

This equation can be rewritten in matrix form as

$$\vec{L} = I\vec{\omega} \tag{3.26}$$

where I is the moment of inertia tensor and its components depend on $\vec{\rho_i}$ and m_i

3.2.6 Dynamic Equations of Motion

In an inertial coordinate system, the dynamic equation of movement is 3.6. Therefore, applying equation 3.19 to get the equation in the body frame $(\cdot)_B$, yields

$$\left(\frac{\delta \vec{L}}{\delta t} \right)_B = -\omega \wedge \vec{L} + \left(\frac{\delta \vec{L}}{\delta t} \right)_I = -\omega \wedge \vec{L} + \left(\vec{N} \right)_B \tag{3.27}$$

From now on, we will omit the subscript B because of simplicity. Now, taking into account the equation 3.26, we have

$$\boxed{I \frac{\delta \vec{\omega}}{\delta t} = \vec{N} - \omega \wedge \left(I\vec{\omega} \right)} \tag{3.28}$$

3.3 Magnetic Field

The Earth Magnetic Field can be represented as the gradient of the scalar potential function V[78]

$$V(R,\theta_R,\lambda_R) = \\ = R_e \sum_{n=1}^{k} \left(\frac{R_e}{R}\right)^{n+1} \sum_{m=0}^{n} \left(g_n^m \cos m\lambda_R + h_n^m \sin m\lambda_R\right) P_n^m(\cos\theta_R) \tag{3.29}$$

Thus,

$$\vec{B} = -\nabla V \tag{3.30}$$

where R_e is the equatorial radius of the Earth (6371.2 adopted for the international Geomagnetic Field, IGRF); g_n^m and h_n^m are Gaussian coefficients[1]; and R, θ_R and λ_R are the geocentric distance, co-elevation, and East longitude from Greenwich which define any point in space. P_n^m is the associated Legendre function of the first kind of degree n and order m:

$$P_n^m(x) = \frac{\left(1-x^2\right)^{m/2}}{2^n \cdot n!} \frac{\delta^{n+m}}{\delta x^{n+m}} \left(x^2-1\right)^n \tag{3.31}$$

These equations give a complete framework for simulation purposes. However, for analytic purposes, it is convenient to obtain a *dipole model* by expanding the field model to first degree (n=1) and all orders (m=0,1). Then, eq. 3.29 becomes:

$$\begin{aligned} V(R,\theta_R,\lambda_R) &= \frac{R_e^3}{R^2}\left[g_1^0 P_1^0(\cos\theta_R) + \left(g_1^1\cos\lambda_R + h_1^1\sin\lambda_R\right) P_1^1(\cos\theta_R)\right] \\ &= \frac{R_e^3}{R^2}\left(g_1^0\cos\theta_R + g_1^1\cos\lambda_R\sin\theta_R + h_1^1\sin\lambda_R\sin\theta_R\right) \end{aligned} \tag{3.32}$$

The $\cos\theta$ term is just the potential due to a dipole of strength $g_1^0 R_e^3$ aligned with the polar axis. Similarly, the $\sin\theta$ terms are dipoles

[1]The IGRF coefficients can be consulted in `http://www.ngdc.noaa.gov/IAGA/vmod/igrf.html`

aligned with the x and y axes. Relying on the principle of linear superposition, these terms are just the Cartesian components of the dipole component of the Earth's magnetic field. For 2010:

$$\begin{aligned} g_1^0 &= -29496.5 \\ g_1^1 &= -1585.9 \\ h_1^1 &= 4945.1 \end{aligned}$$

Therefore, the total dipole strength is:

$$R_e^3 H_0 = R_e^3 \sqrt{\left[\left(g_1^0\right)^2 + \left(g_1^1\right)^2 + \left(h_1^1\right)^2 \right]} = 7.746 \times 10^{15} Wb \cdot m \quad (3.33)$$

The coelevation of the dipole is

$$\theta'_m = \arccos\left(\frac{g_1^0}{H_0}\right) = 170.0^\circ \quad (3.34)$$

The East longitude of the dipole is

$$\phi'_m = \arctan\left(\frac{h_1^1}{g_1^1}\right) = 107.8^\circ \quad (3.35)$$

Now we can approximate the magnetic field of the Earth as due to a vector dipole, $\vec{m}$, whose magnitude and direction are given by eqs. 3.33 to 3.35. Thus,

$$\vec{B}\left(\vec{R}\right) = R_e^3 H_0 \left[\frac{3\left(\vec{m}\cdot\vec{R}\right)\vec{R}}{\left\|\vec{R}\right\|^5} - \frac{\vec{m}}{\left\|\vec{R}\right\|^3} \right] \quad (3.36)$$

Where $\vec{R}$ is the position vector of the point at which the field is desired.

3.3.1 Dipole and full Model

As described before, The dipole model is the full model implemented up to order 1. However, the model provides coefficients up to order

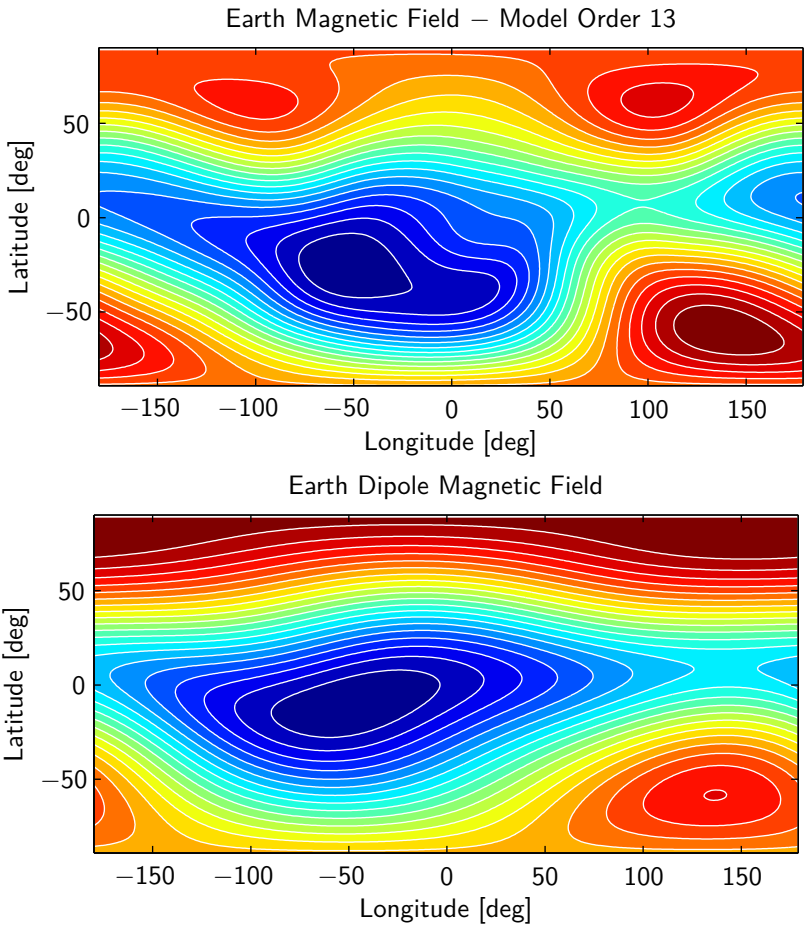

Figure 3.2: Magnetic Models at 100 Km

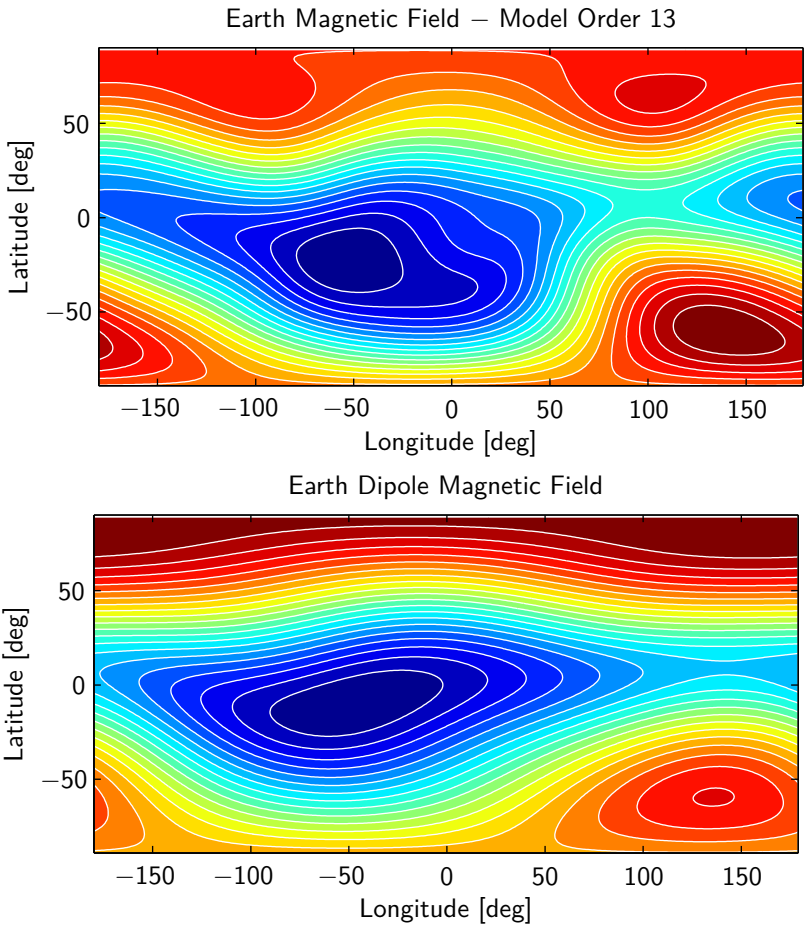

Figure 3.3: Magnetic Models at 500 Km

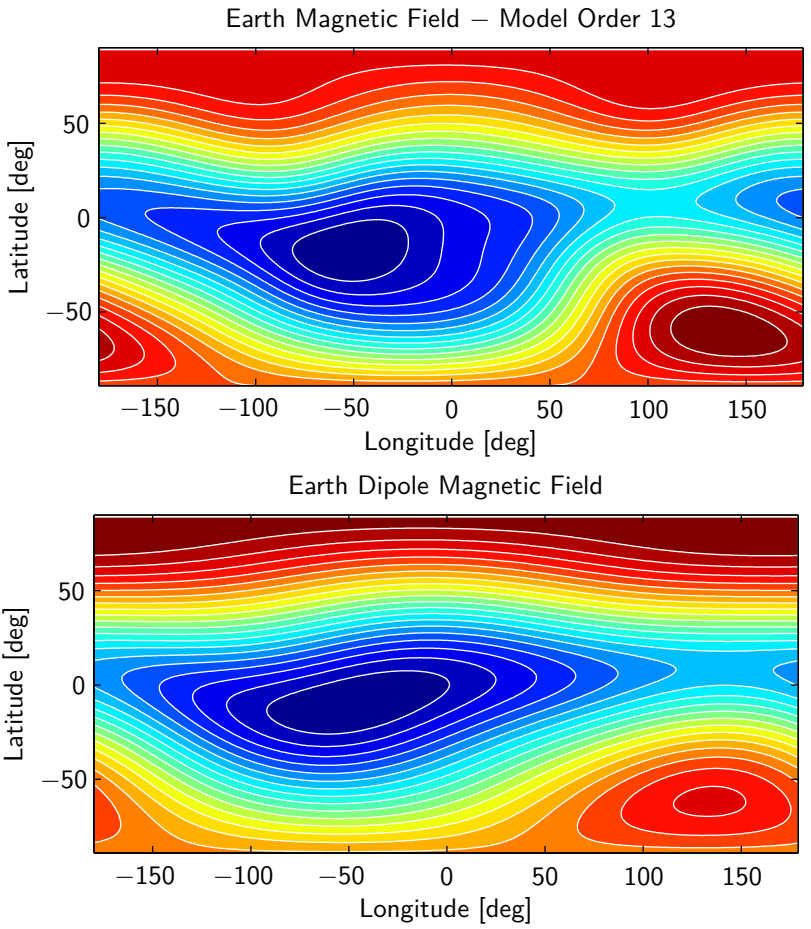

Figure 3.4: Magnetic Models at 1500 Km

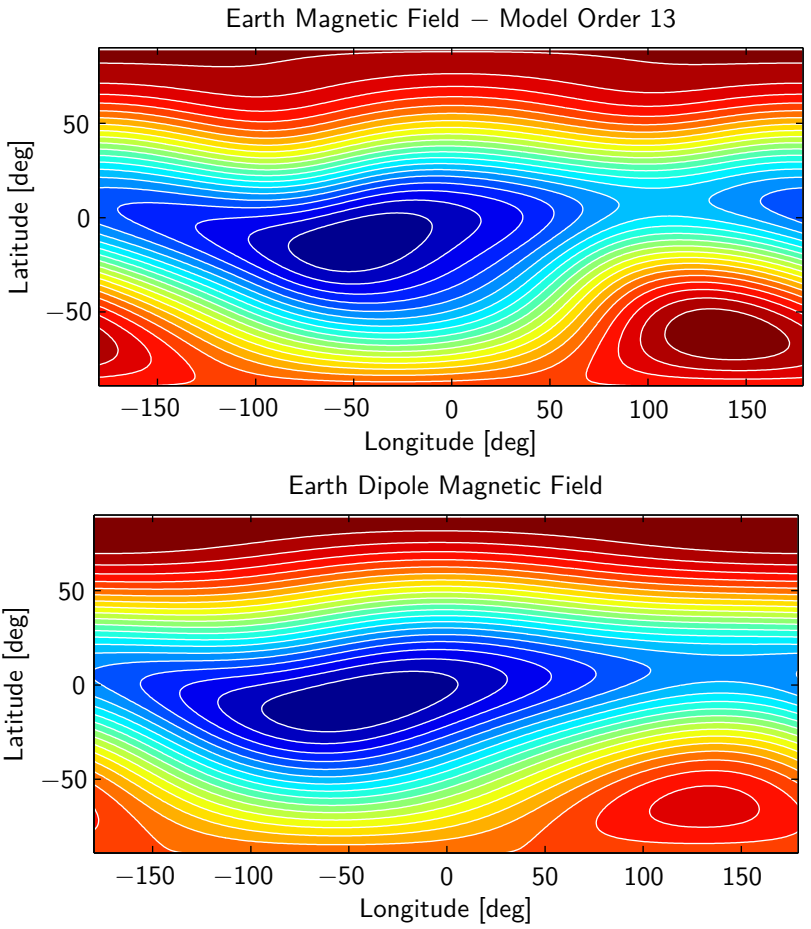

Figure 3.5: Magnetic Models at 3000 Km

13. In figures 3.2 to 3.5, several plots comparing the dipole model with the full model are presented.

The coefficients in the order one are the most significant, therefore the dipole described by these coefficients becomes dominant at larger distances. It is important to notice that at lower altitude the difference between the dipole model and the order 13th model (which is closer to the real Earth magnetic field) are much higher than at higher altitude. However, the order of the model that is precise enough for each application depends on the altitude at which the satellite is orbiting. In figure 3.6 the field lines of the magnetic field of the Earth are represented.

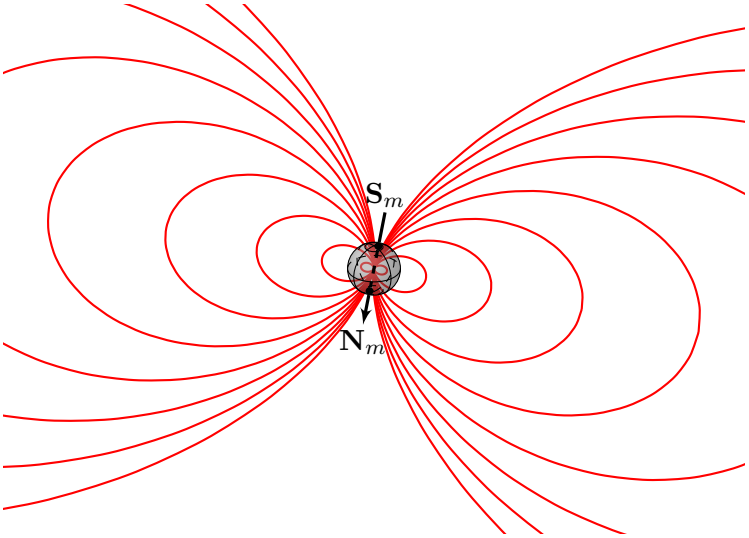

Figure 3.6: Earth dipole Magnetic Field

3.4 State-Dependent Coefficients (SDC) factorization

Merging in one single model the attitude dynamics equations of motion, the kinematics and the dipole model of the magnetic field, the system dynamics can be factorized in State Dependent Coefficients

(SDC) form:

$$\dot{x} = A(x)\,x + B(x)\,u \tag{3.37}$$

where A models the spacecraft system dynamics and B models the actuators effect.

Let $x = \left[\omega_{pi}^T, q_v^T\right]^T$ be the state vector. A reduced quaternion q_v is considered to describe the kinematics[79] :

$$\begin{bmatrix} \dot{q_1} \\ \dot{q_2} \\ \dot{q_3} \end{bmatrix} = \frac{1}{2} \begin{bmatrix} q_0 & -q_3 & q_2 \\ q_3 & q_0 & -q_1 \\ -q_2 & q_1 & q_0 \end{bmatrix} \cdot \begin{bmatrix} \omega_1 \\ \omega_2 \\ \omega_3 \end{bmatrix} \tag{3.38}$$

where q_0 is substituted by $\sqrt{1 - q_1^2 - q_2^2 - q_3^2}$.

Equation (3.28) can be rewritten using the property $a \wedge b = S(a) \cdot b$ where $S(\cdot)$ is defined as the operator which obtains the skew-symmetric matrix using the coefficients of a given vector (See appendix A). Let $a = [a_1, a_2, a_3]^T$. Then:

$$S(a) = \begin{bmatrix} 0 & -a_3 & a_2 \\ a_3 & 0 & -a_1 \\ -a_2 & a_1 & 0 \end{bmatrix} \tag{3.39}$$

There are several options to factorize the non-linear problem into the SDC form. Among the possible, the following form has been selected:

$$A = \begin{bmatrix} A_{11} & A_{12} \\ A_{21} & 0 \end{bmatrix} \tag{3.40}$$

$$\begin{aligned} A_{11} = &- S(A_{lvlh}^{pi}\omega_{lvlh}) - I^{-1} \cdot S(w_{pi}) \cdot I + \\ &+ I^{-1} \cdot S(I \cdot A_{lvlh}^{pi}\omega_{lvlh}) - I^{-1} \cdot S(A_{lvlh}^{pi}\omega_{lvlh}) \cdot I \end{aligned}$$

$$A_{12} = \begin{bmatrix} 2\xi\omega_{orb}^2 q_0 \frac{Iyy-Izz}{Ixx} & 0 & 2\xi\omega_{orb}^2 q_2 \frac{Iyy-Izz}{Ixx} \\ 0 & 2\xi\omega_{orb}^2 q_0 \frac{Ixx-Izz}{Iyy} & 2\xi\omega_{orb}^2 q_1 \frac{Izz-Ixx}{Iyy} \\ -4\omega_{orb}^2 \frac{Ixx-Iyy}{Izz}\zeta q_0 & 0 & -4\omega_{orb}^2 \frac{Ixx-Iyy}{Izz}\zeta q_2 \end{bmatrix}$$

$$A_{21} = \frac{1}{2}\left[S(q_v) + q_0 I_3\right]$$

where $\xi = q_0^2 - q_1^2 - q_2^2 + q_3^2$, $\zeta = q_0 q_2 - q_1 q_3$ and I_3 is the identity matrix of order 3. Matrix B becomes:

$$B = -I^{-1} S(\beta_{pi}) \tag{3.41}$$

where β_{pi} is the Magnetic field in the principal axis reference frame. To calculate β_{pi} equation 3.36 is used. This is a vectorial equation that is valid in whatever reference frame that is used, provided that both R and m are centered in the reference system. As a circular orbit has been considered, R is very easy to calculate in the Orbit reference system:

$$R_{lnb} = R_{orbit} \begin{bmatrix} \cos(\theta_p) \\ \sin(\theta_p) \\ 0 \end{bmatrix} \tag{3.42}$$

where θ_p is the satellite anomaly. The orientation of the magnetic dipole can be derived using standard rotations. Therefore:

$$m_{lnb} = \begin{bmatrix} \sin(\theta'_m) \cdot \cos(\Omega - \alpha_m) \\ -\sin(\theta'_m) \cdot \cos(i) \cdot \sin(\Omega - \alpha_m) + \cos(\theta'_m) \cdot \sin(i) \\ \sin(\theta'_m) \cdot \sin(i) \cdot \sin(\Omega - \alpha_m) + \cos(\theta'_m) \cdot \cos(i) \end{bmatrix} \tag{3.43}$$

where Ω is the Right Ascension of the Ascending Node (RAAN), i is the orbit inclination and $\alpha_m = \phi'_m + \alpha_G$. α_G is the angle of rotation of the Earth and θ'_m and ϕ'_m are given by equations (3.34) and (3.35). Substituting equations 3.42 and 3.43 into equation 3.36, the magnetic field in the Orbit Perifocal frame (B_{lnb}) is given. Thus, β_{pi} is:

$$\beta_{pi} = A_{lnb}^{pi} \cdot B_{lnb} \tag{3.44}$$

where A_{lnb}^{pi} is the transformation matrix between the Orbit Perifo-

cal reference frame and the Principal Inertia frame and is given by:

$$A_{lnb}^{pi} = \left[(q_0^2 - q_v^T q_v)I_3 + 2q_v q_v^T - 2q_0 S(q_v)\right] \begin{bmatrix} \cos(\theta_P) & \sin(\theta_P) & 0 \\ -\sin(\theta_P) & \cos(\theta_P) & 0 \\ 0 & 0 & 1 \end{bmatrix} \tag{3.45}$$

Different factorizations of the model are possible. The factorization has an effect on the efficiency of the control algorithm[80]. However the study of the effects of different factorizations is not discussed in this work. It is pointed out as an open research topic in chapter 7.

3.5 Description of the Applied Control Technique (ASRE)

In the previous section, the model is written in State-Dependent Coefficient form. This equation is a common non linear equation. One solution to the control problem given by this equation is the State-Dependent Riccati Equation (SDRE) strategy[81]. Its solution is well-known and has became very popular within the control community over the last decade[80].

Consider the general infinite-horizon, input-affine, autonomous, nonlinear regulator problem of the form:

Minimize

$$J = \frac{1}{2}\int_{t_0}^{\infty} z^T z + u^T R(x) u \delta t \tag{3.46}$$

with respect to the state $\vec{x}$ and control $\vec{u}$ subject to the nonlinear systems constraints

$$\dot{\vec{x}} = A(\vec{x}) + B(\vec{x})\,\vec{u} \tag{3.47}$$

$$\dot{\vec{z}} = C(\vec{x}) \tag{3.48}$$

where $x \in R^n$, $u \in R^m$ and $z \in R^s$, and where $R(x) \gg 0$ for all

x. We assume that $F(0) = 0$ and that $B(x) \neq 0$ in a neighborhood around the origin

The SDRE approach for obtaining a suboptimal solution of problem 3.46–3.48 is

1. Use direct parametrization to bring the nonlinear dynamics to the state-dependent coefficient (SDC) form

$$\dot{x} = A(\vec{x})\,\vec{x} + B(\vec{x})\,\vec{u} \tag{3.49}$$

   where

$$f(\vec{x}) = A(\vec{x})\,\vec{x} \tag{3.50}$$

2. Solve the state-dependent Riccati equation

$$A^T(\vec{x})\,P + PA(\vec{x}) - PB(\vec{x})\,R^{-1}(\vec{x})\,B^T(\vec{x})\,P + C^T(\vec{x})\,C(\vec{x}) = 0 \tag{3.51}$$

   to obtain $P \geq 0$ where P is a function of x.

3. Construct the nonlinear feedback controller

$$u = -R^{-1}(\vec{x})\,B^T(\vec{x})\,P(\vec{x})\,\vec{x} \tag{3.52}$$

Therefore, the nonlinear system is approximated by a linear one and solved as a LQR problem at each sample time.

However, the matrix B depends on the state $x = \left[\omega_{pi}^T, q_v^T\right]^T$, on the satellite anomaly (θ_p) and on the angle of rotation of the Earth (α_G). The latter two parameters are not constant and depend on time by the equations 3.53 and 3.54.

$$\theta_p = \omega_{orb} \cdot t + \theta_{p0} \tag{3.53}$$

$$\alpha_G = \omega_{Earth} \cdot t + \alpha_{G0} \tag{3.54}$$

It is difficult to introduce these equations in a state space model differential equation. One possible model of this dynamic system is

given by equations 3.55 and 3.56, and the state-space representation is given by 3.57 and 3.58.

$$\dot{\theta_p} = \omega_{orb} \tag{3.55}$$

$$\dot{\alpha_G} = \omega_{Earth} \tag{3.56}$$

$$\begin{bmatrix} \ddot{\theta_p} \\ \dot{\theta_p} \\ \ddot{\alpha_G} \\ \dot{\alpha_G} \end{bmatrix} = \begin{bmatrix} 0 & 0 & 0 & 0 \\ 1 & 0 & 0 & 0 \\ 0 & 0 & 0 & 0 \\ 0 & 0 & 1 & 0 \end{bmatrix} \begin{bmatrix} \dot{\theta_p} \\ \theta_p \\ \dot{\alpha_G} \\ \alpha_G \end{bmatrix} \tag{3.57}$$

$$\vec{x_0} = \begin{bmatrix} \omega_{orb} \\ \theta_{p0} \\ \omega_{Earth} \\ \alpha_{G0} \end{bmatrix} \tag{3.58}$$

This system is not controllable. In fact, it is a reduced model of a free dynamic that has effect on the system to control but no variable to be controlled. Furthermore, the state $\vec{x} = [0\ 0\ 0\ 0]^T$ does not represent a physical state.

The more important property of SDRE that made its use not useful for attitude control using only magnetorquers is derived from its linear point-wise division. As described in [80] or in [82], the pair $\{A(\vec{x}), B(\vec{x})\}$ used in the SDRE formulation should be tested for controllability over the entire state trajectory. However, due to the lack of one degree of freedom in magnetorquers actuated spacecraft, the state space parametrization must be changed to fulfill this condition. Therefore, this problem cannot be solved by an SDRE controller.

The state space nonlinear system dynamics is better described by

$$\dot{x} = A\left(x, t\right) x + B\left(x, t\right) u \tag{3.59}$$

This model can be used to solve a nonlinear control problem, formulated as to minimize the nonlinear objective function of the form

$$J = \frac{1}{2}x^T(t_f)S\left(x(t_f), t_f\right)x(t_f) + \frac{1}{2}\int_{t_0}^{t_f} x^T Q\left(x,t\right)x + u^T R\left(x,t\right)u\ dt \tag{3.60}$$

where S, Q are two positive-semidefinite matrices and R is a 3x3 positive definite matrix.

This type of problems are non-linear *time varying* problems, because the state space representation still depends on time. The Approximating Sequence of Riccati Equations (ASRE) technique can deal with this type of problems[83]. This method has been used in the literature to solve nonlinear control problems [84][85].

ASRE is based on transforming the problem given by equations 3.59-3.60 into an equivalent time variant problem with the introduction of the iterative sequence corresponding to the system dynamics:

$$\dot{x}^0(t) = A(x_0,t)x^0(t) + B(x_0,t)u^0(t)$$

$$\dot{x}^i(t) = A(x^{i-1}(t),t)x^i(t) + B(x^{i-1}(t),t)u^i(t) \tag{3.61}$$

$$x^i(t_0) = x_0 \quad i = 1,\ldots,N$$

and the iterative sequence corresponding to the cost function to be minimized:

$$J^i = \frac{1}{2}x^{iT}(t_f)Sx^i(t_f) + \frac{1}{2}\int_{t_0}^{t_f} x^{iT}Q\left(x^{i-1},t\right)x^i + u^{iT}R\left(x^{i-1},t\right)u^i\ dt \tag{3.62}$$

The problem described by Equations 3.61 and 3.62 can be solved as a sequence of *Two Points Boundary Value Problem* using the costate transformation. Furthermore, the final state of the problem is not fixed. Instead the algorithm tries to minimize $x^{iT}(t_f)Sx^i(t_f)$. This

iterative method is described in detail in Reference [86] as a Soft Constrained Problem (SCP). The Hamiltonian of this problem is

$$H = \frac{1}{2}\left[\mathbf{x}^T Q(t)\mathbf{x} + \mathbf{u}^T R(t)\mathbf{u}\right] + \boldsymbol{\lambda}^T\left[A(t)\mathbf{x} + B(t)\mathbf{u}\right], \tag{3.63}$$

and the optimality conditions read

$$\dot{\mathbf{x}} = A(t)\mathbf{x} + B(t)\mathbf{u}, \tag{3.64}$$

$$\dot{\boldsymbol{\lambda}} = -Q(t)\mathbf{x} - A^T(t)\boldsymbol{\lambda}, \tag{3.65}$$

$$0 = R(t)\mathbf{u} + B^T(t)\boldsymbol{\lambda}. \tag{3.66}$$

From equation (3.66) it is possible to get

$$\mathbf{u} = -R^{-1}(t)B^T(t)\boldsymbol{\lambda}, \tag{3.67}$$

which can be substituted into (3.64)–(3.65) to yield

$$\dot{\mathbf{x}} = A(t)\mathbf{x} - B(t)R^{-1}(t)B^T(t)\boldsymbol{\lambda}, \tag{3.68}$$

$$\dot{\boldsymbol{\lambda}} = -Q(t)\mathbf{x} - A^T(t)\boldsymbol{\lambda}. \tag{3.69}$$

In a compact form, equations (3.68)–(3.69) can be arranged as

$$\begin{pmatrix} \dot{\mathbf{x}} \\ \dot{\boldsymbol{\lambda}} \end{pmatrix} = \begin{bmatrix} A(t) & -B(t)R^{-1}(t)B^T(t) \\ -Q(t) & -A^T(t) \end{bmatrix} \begin{pmatrix} \mathbf{x} \\ \boldsymbol{\lambda} \end{pmatrix}. \tag{3.70}$$

Since (3.70) is a system of linear differential equations, the exact solution can be written as

$$\mathbf{x}(t) = \phi_{xx}(t_i, t)\mathbf{x}_i + \phi_{x\lambda}(t_i, t)\boldsymbol{\lambda}_i, \tag{3.71}$$

$$\boldsymbol{\lambda}(t) = \phi_{\lambda x}(t_i, t)\mathbf{x}_i + \phi_{\lambda\lambda}(t_i, t)\boldsymbol{\lambda}_i, \tag{3.72}$$

where the functions ϕ_{xx}, $\phi_{x\lambda}$, $\phi_{\lambda x}$, and $\phi_{\lambda\lambda}$ are the components of the state transition matrix

$$\Phi(t_i, t) = \begin{bmatrix} \phi_{xx}(t_i, t) & \phi_{x\lambda}(t_i, t) \\ \phi_{\lambda x}(t_i, t) & \phi_{\lambda\lambda}(t_i, t) \end{bmatrix}, \tag{3.73}$$

which can be found by integrating the following dynamics

$$\begin{bmatrix} \dot{\phi}_{xx} & \dot{\phi}_{x\lambda} \\ \dot{\phi}_{\lambda x} & \dot{\phi}_{\lambda\lambda} \end{bmatrix} = \begin{bmatrix} A(t) & -B(t)R^{-1}(t)B^T(t) \\ -Q(t) & -A^T(t) \end{bmatrix} \begin{bmatrix} \phi_{xx} & \phi_{x\lambda} \\ \phi_{\lambda x} & \phi_{\lambda\lambda} \end{bmatrix}, \tag{3.74}$$

with initial conditions

$$\begin{aligned} \phi_{xx}(t_i, t_i) &= I_{n\times n}, \quad \phi_{x\lambda}(t_i, t_i) = 0_{n\times n}, \\ \phi_{\lambda x}(t_i, t_i) &= 0_{n\times n}, \quad \phi_{\lambda\lambda}(t_i, t_i) = I_{n\times n}. \end{aligned} \tag{3.75}$$

From Equations (3.71)–(3.75) we can infer that if both $\mathbf{x}_i$ and $\boldsymbol{\lambda}_i$ were given, then it would be possible to achieve $\mathbf{x}(t)$ and $\boldsymbol{\lambda}(t)$, and therefore the optimal control function $\mathbf{u}(t)$ through (3.67). We recall that the initial condition is given; i.e., $\mathbf{x}(t_i) = \mathbf{x}_i$. To compute $\boldsymbol{\lambda}_i$ consider that the final state is not specified, and thus S in equation (3.60) is a $n \times n$ positive definite matrix. The transversality condition sets a relation between the state and costate at final time

$$\boldsymbol{\lambda}(t_f) = S(t_f)\mathbf{x}(t_f), \tag{3.76}$$

which can be used to find $\boldsymbol{\lambda}_i$. This is done by writing (3.71)–(3.72) at final time and substituting relation (3.76)

$$\mathbf{x}(t_f) = \phi_{xx}(t_i, t_f)\mathbf{x}_i + \phi_{x\lambda}(t_i, t_f)\boldsymbol{\lambda}_i, \tag{3.77}$$

$$S(t_f)\mathbf{x}(t_f) = \phi_{\lambda x}(t_i, t_f)\mathbf{x}_i + \phi_{\lambda\lambda}(t_i, t_f)\boldsymbol{\lambda}_i. \tag{3.78}$$

Equations (3.77)–(3.78) represent a linear algebraic system of $2n$ equations in the $2n$ unknowns $\{\mathbf{x}(t_f), \boldsymbol{\lambda}_i\}$. The system can be solved by substitution to yield

$$\begin{aligned} \boldsymbol{\lambda}_i(\mathbf{x}_i, t_i, t_f) = &\left[\phi_{\lambda\lambda}(t_i, t_f) - S(t_f)\phi_{x\lambda}(t_i, t_f)\right]^{-1} \cdot \\ &\cdot \left[S(t_f)\phi_{xx}(t_i, t_f) - \phi_{\lambda x}(t_i, t_f)\right]\mathbf{x}_i. \end{aligned} \tag{3.79}$$

The procedure requires inverting the $n \times n$ matrix

$$\phi_{\lambda\lambda}(t_i, t_f) - S(t_f)\phi_{x\lambda}(t_i, t_f)$$

3.6 Conclusions of this chapter

In this chapter all the equations used in the modeling and the solution of the problem are presented. A possible factorization of a nadir

pointing attitude control system is presented in section 3.4. Furthermore, the Approximating Sequence of Riccati Equation technique is presented to solve the nonlinear problem of a nadir pointing spacecraft under exclusive magnetic control torque. The proposed attitude control system is capable of controlling a nadir pointing spacecraft with the performance described in the next chapter.

4

Simulations and Results

This chapter presents the simulation results of the attitude control system presented in chapter 3. First, the simulation environment is described in section 4.1. All assumptions and perturbation models are discussed. In section 4.2, a comparison of the performance of the control system is presented for small and large initial conditions and under the effects of perturbations and model uncertainties. Finally, in section 4.3 an analysis of the performance of the control system for different orbits is presented.

4.1 Simulation Environment

In order to validate the control algorithm for a test satellite, a simulation environment has been set up in Matlab/Simulink. The ASRE is implemented in Matlab scripts and the orbit and attitude propagation have been developed by using Simulink.

The control algorithm described in section 3.5 can solve the problem in a given horizon time. The calculated control outputs are stored and then time-triggered output. It is not efficient at all to solve the problem for a whole orbit, because the simulated state will not match the real state due to perturbation or model uncertainties. Therefore a Time-Span (TS) parameter is defined. The time span is the length in seconds of the period where the control is calculated. Thus, the control will be calculated in every time-span period. An schematic state diagram of simulation algorithm is presented in figure 4.1.

The satellite under test is an imaginary satellite whose numerical parameters for the orbit and inertia properties of the satellite are representative of a small satellite in a LEO orbit. These parameters have been chosen for a preliminary test of the control algorithm. Specifically, the inertia moments of the satellite are:

$$\begin{aligned} I_{xx}&=1.0\ [kg \cdot m^2] \\ I_{yy}&=1.2\ [kg \cdot m^2] \\ I_{zz}&=1.5\ [kg \cdot m^2] \end{aligned} \tag{4.1}$$

The orbit parameters are:

$$\begin{aligned} i&=90 \cdot pi/180\ [rad] \\ \Omega&=180\ [rad] \\ R_{orbit}&=R_{Earth} + 500\ [km] \end{aligned} \tag{4.2}$$

Given the inertia and orbit parameters of the spacecraft, the performance of the control system will be highly dependent on the way the performance index is defined (Equation 3.62) and on the control time span $t_f - t_0$. For the case under consideration, a control time

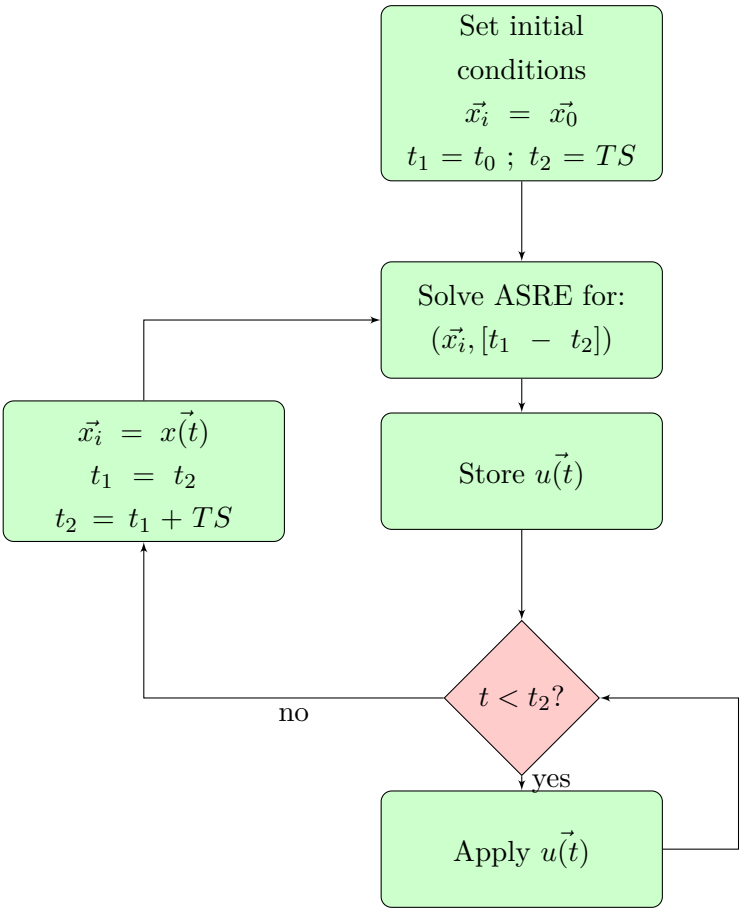

Figure 4.1: Simulation flow chart

span of 5 seconds has been adopted, which means that one orbit is covered in 1160 time spans.

The matrices Q, S and R have been chosen as:

$$S = Q = diag\left(\begin{bmatrix} \frac{1}{\bar{\omega}^2} & \frac{1}{\bar{q}^2} \end{bmatrix}\right) \quad R = I_3 \tag{4.3}$$

where $\bar{w} = \omega_{orb}$ is the value of the nominal angular velocity in pitch and $\bar{q} = \sin(3\pi/180)$ is the quaternion value for an angle of 3 degrees. This choice, common in the definition of optimal control problems, assumes that:

- equal importance is given to each axis;
- three degrees angular error and angular velocity error equal to the nominal pitch angular velocity are the maximum admissible;
- the maximum dipole moment generated by the actuators should be 1 $[A \cdot m^2]$, that is within the performances of commercial magnetic actuators for this class of satellites.

A sample simulation with the initial conditions in 4.4 is performed, where the results are shown in figures 4.2 to 4.5.

$$\begin{bmatrix} \phi \\ \theta \\ \psi \end{bmatrix} = \begin{bmatrix} 10 \\ 5 \\ -3 \end{bmatrix} \quad ; \quad \begin{bmatrix} \omega_1 \\ \omega_2 \\ \omega_3 \end{bmatrix} = \begin{bmatrix} 0 \\ 0 \\ 0 \end{bmatrix} \tag{4.4}$$

In figure 4.2, the attitude error angles with respect to the nadir pointing attitude are represented. In figure 4.3, the same error is represented in quaternion form. As explained in section 3.2, the attitude error can be described using angles or using quaternions, both are equivalent. Therefore, figures 4.2 and 4.3 are redundant. Angles are better for representation because they have a physical meaning, however the system attitude and control is written using quaternions. Both representations will be used.

The results in figures 4.2 to 4.5 show that the control algorithm is able to stabilize the satellite in a few orbits. Another particularity of

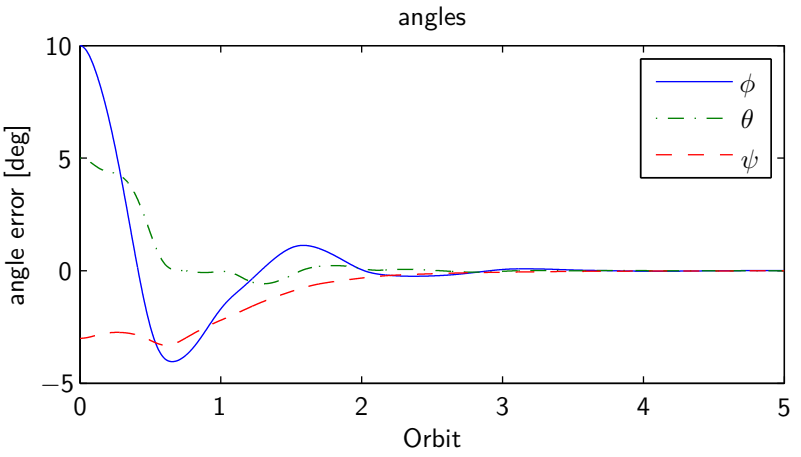

Figure 4.2: Angle Errors

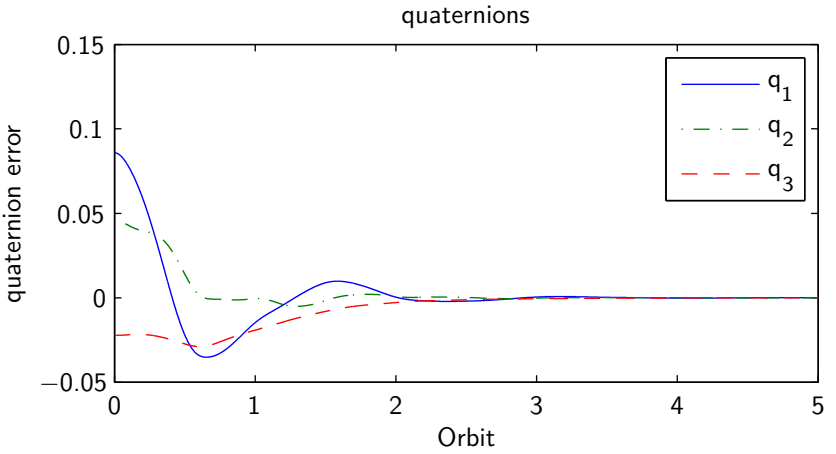

Figure 4.3: Quaternion Error

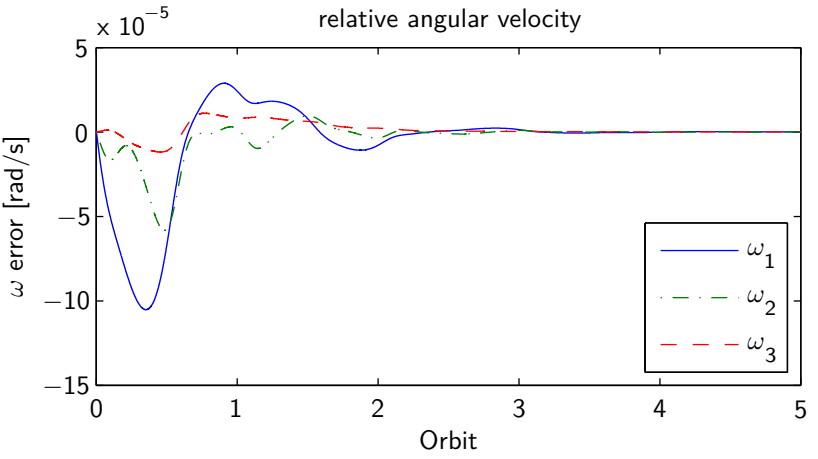

Figure 4.4: ω Error

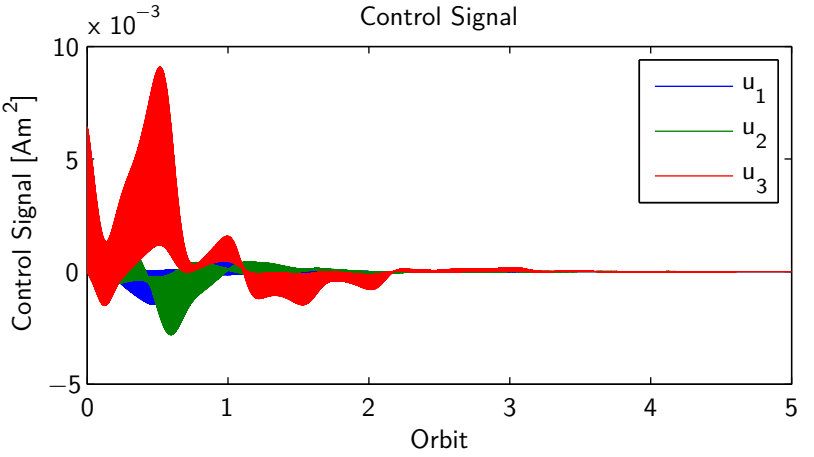

Figure 4.5: Control Signal

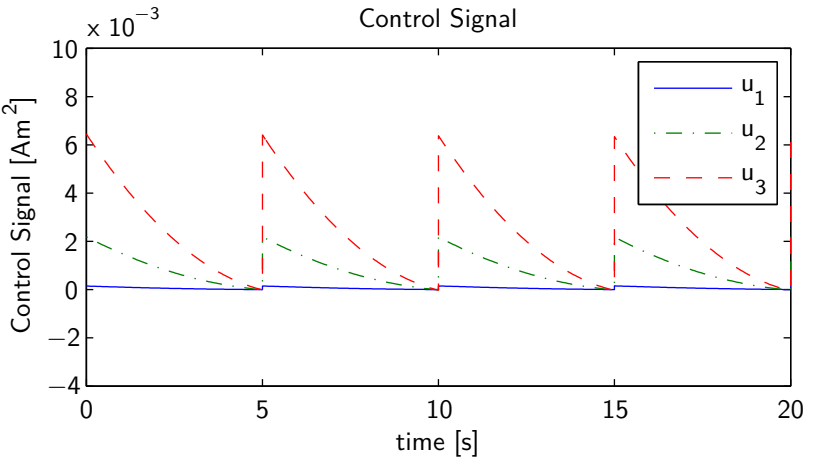

Figure 4.6: Control Detail

this type of control is the kind of control signal that is applied to the satellite. A control signal is calculated in every time span. A zoom on the first 20 seconds of the control signal is represented in figure 4.6. This figure shows in detail how the control signal is generated and applied within each time span. Every 5 seconds the control problem defined by Equations 3.61 and 3.62 is solved with initial conditions equal to the final conditions at the end of the previous time span, as is described in figure 4.1.

4.2 Perturbation Analysis

Simulations have been performed first with small error on the initial conditions and then with large initial conditions which might be the result of a detumbling using control techniques such as Bdot.

Two main disturbance sources have been considered for the simulation environment. First, a model uncertainty has been introduced. As described before in section 3.3, the Earth magnetic field can be reproduced very accurately with the model introduced by the equations (3.29) to (3.31). However, only the first grade of the polynomial,

which is equal to a dipole, is taken into account in the control design. Therefore as an example of model uncertainty a 13th order polynomial has been introduced in the simulation as the real magnetic field seen by the spacecraft. The module of the Earth magnetic field modeled by the dipole and by 13th order model are shown in figure 4.7 for an orbit of 89 degrees of inclination and at an altitude of 500km.

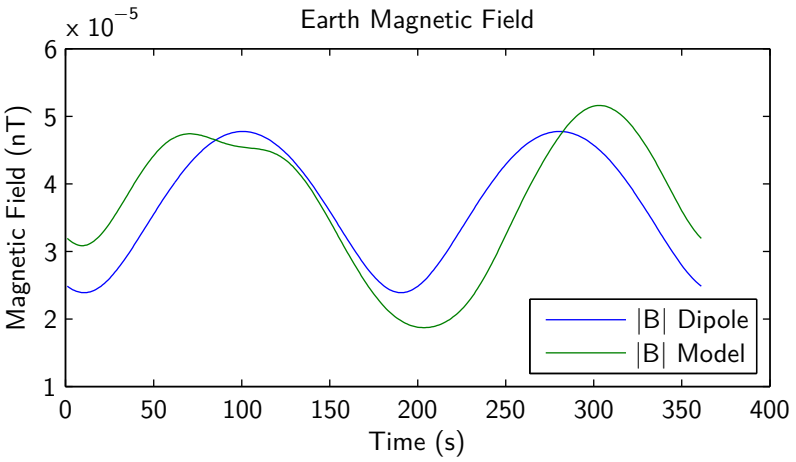

Figure 4.7: Module of the magnetic field during one orbit

As described in section 3.3, the error between the magnetic field dipole model and higher order model decrease with altitude. The error also depends on RAAN. These properties are shown in figure 4.8, where the error of the dipole model and the full model for different altitudes and RAAN is presented. Then, the error introduced as a model uncertainty depends on altitude and RAAN.

Thus, the results obtained for a given setup of the control algorithm will also depend in the orbit properties.

Second, gravity gradient is introduced in the simulation. Gravity gradient effects and equations are described in section 2.2.2. It is considered to produce a disturbance torque because the gravity effects are not considered in the control model.

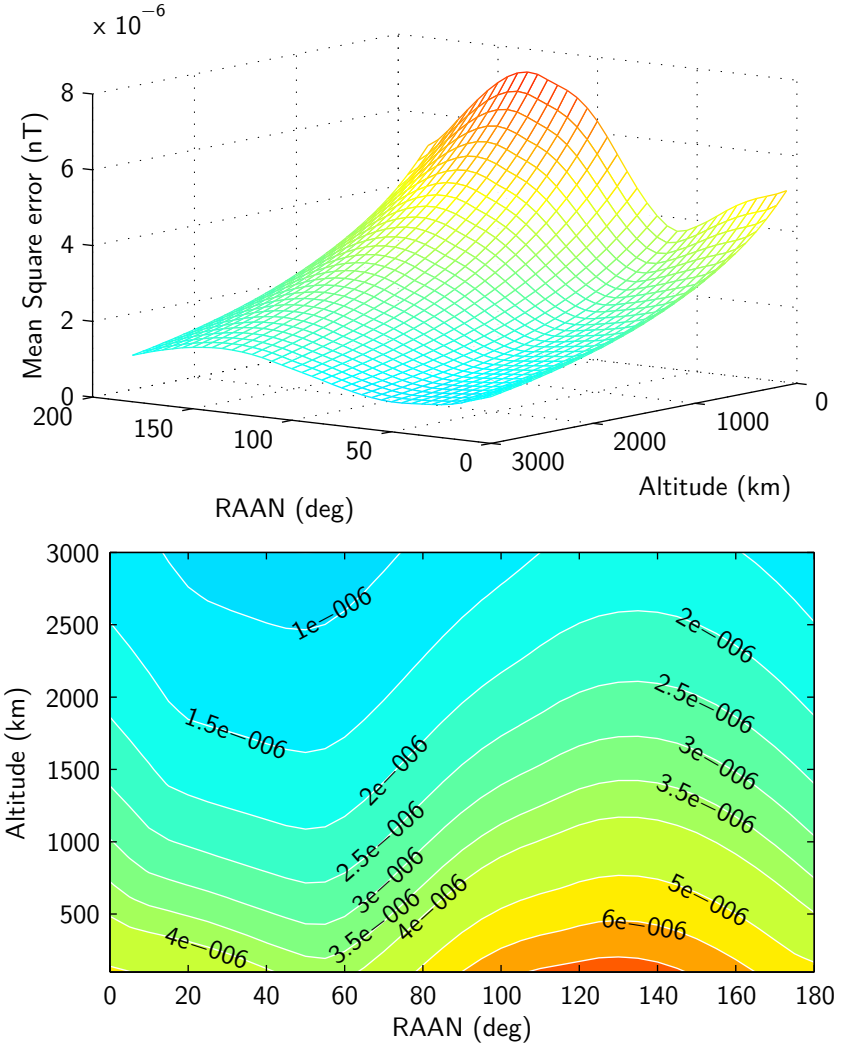

Figure 4.8: Mean square error between dipole and full mode

4.2.1 Small Initial conditions

The initial conditions for these simulations are zero error for angular velocity and an error in the target nadir pointing attitude of 2 degrees in roll, 1 degree in yaw and 0 degrees in pitch, the axis of the nominal angular velocity.

$$\begin{bmatrix} \phi \\ \theta \\ \psi \end{bmatrix} = \begin{bmatrix} 2 \\ 1 \\ 0 \end{bmatrix} \quad ; \quad \begin{bmatrix} \omega_1 \\ \omega_2 \\ \omega_3 \end{bmatrix} = \begin{bmatrix} 0 \\ 0 \\ 0 \end{bmatrix} \tag{4.5}$$

The orbit have been chosen to be one with low inclination for this type of control. It means that the convergence of the algorithm will be slow compared with other orbits as will be presented in the next section. The orbit properties are:

$$\begin{aligned} i{=}15 \cdot pi/180\ [rad] \\ R_{orbit}{=}R_{Earth} + 600\ [km] \end{aligned} \tag{4.6}$$

A simulation of the behavior of the system has been performed for 10 orbits. For the whole control period the control algorithm has reached convergence in at most two iterations. The results of the simulations are shown in Figures from 4.9 to 4.11.

Both figures 4.9 and 4.10 show a good performance for the algorithm in these conditions. In this case perturbations and model uncertainties contribute with some benefit to the stabilization of the satellite, specially in the yaw axis. It is specially difficult for the algorithm to generate a torque for a fine pointing of the yaw axis due to the small value of the magnetic field in a 15 degrees inclination orbit plane. In fact, the magnetic field is almost perpendicular to this orbit.

The maximum value of the control signal in figure 4.11 demonstrates that the control actions are well within the target limits assumed in a small satellite. For instance, the torquerods manufactured by Microcosm/Zarm can produce up to $15Am^2$ for a 33cm rod[1].

[1] `http://www.smad.com/analysis/torquers.pdf`

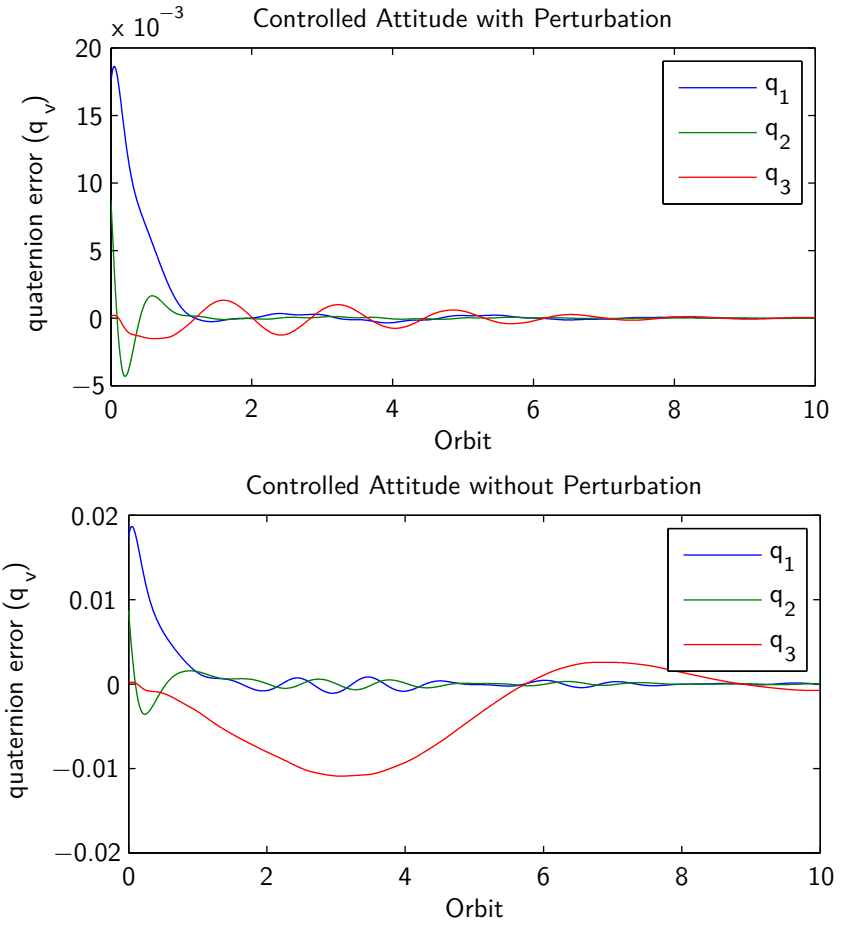

Figure 4.9: Attitude quaternion error

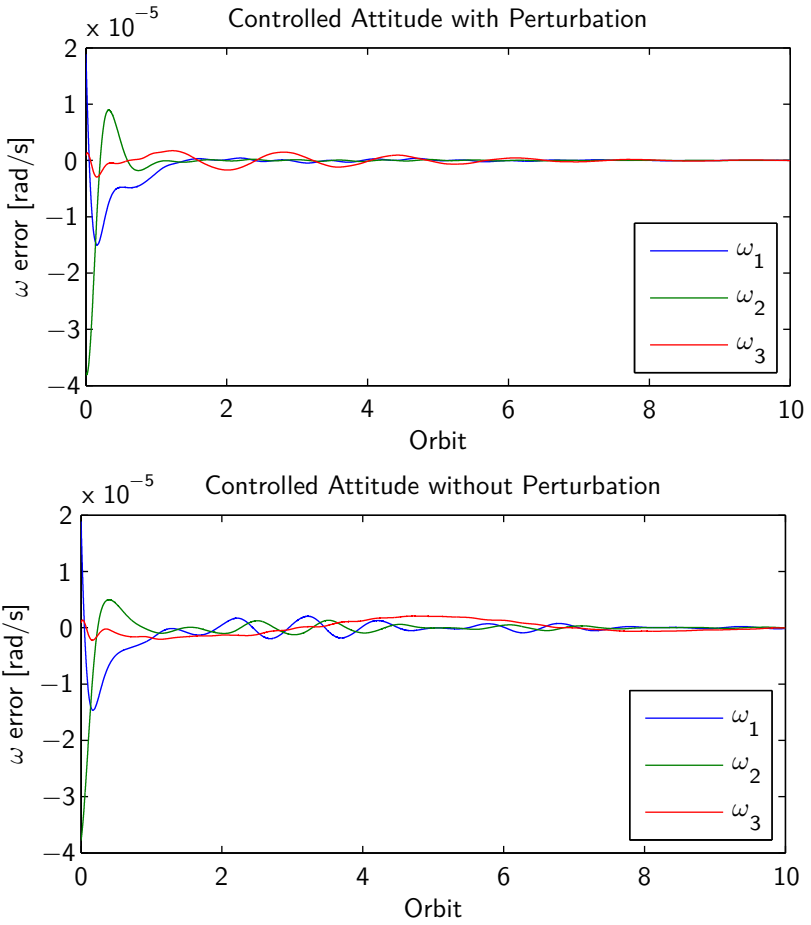

Figure 4.10: Angular velocity error

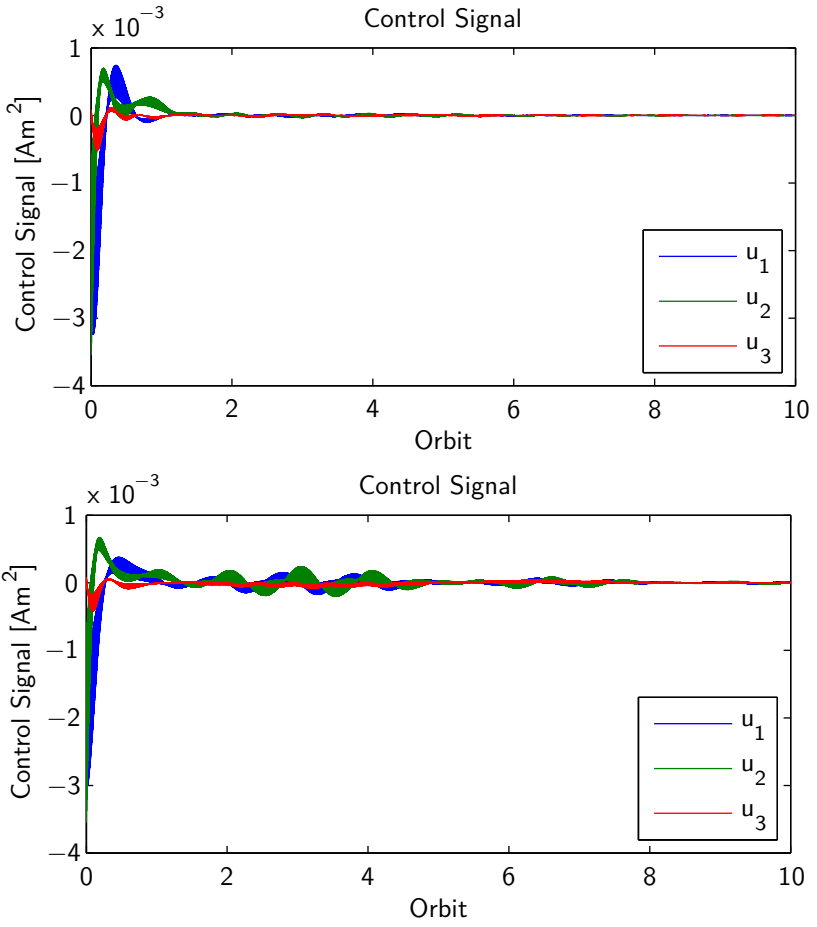

Figure 4.11: Envelope of the Control Signal

4.2.2 Large Initial conditions

Another set of simulations has been carried out in order to test the behavior of the attitude control system in more realistic conditions. Such condition are chosen as a set of large pointing errors and large angular velocities that may result at the end of detumbling phase with a B-dot like algorithm (see section 2.3.3). The B-dot algorithm can usually carry the spacecraft to a total angular rate in the order of two times the nominal angular rate of the nadir pointing spacecraft, this is, two times the orbital angular rate. To be conservative, initial angular rates which are an order of magnitude higher than required have been chosen.

Orbit parameters are the same as with small initial conditions, and are presented in equation 4.6. Initial conditions are shown in equation 4.7.

$$\begin{bmatrix} \phi \\ \theta \\ \psi \end{bmatrix} = \begin{bmatrix} 180 \\ 20 \\ 60 \end{bmatrix} [deg] \quad ; \quad \omega_{ini} = \begin{bmatrix} 0.06 \\ 0.08 \\ 0.05 \end{bmatrix} [rad/s] \tag{4.7}$$

In these conditions, the results of the simulations are presented in figures 4.12 to 4.14 with and without perturbations. Although the initial conditions in angular velocity are large, the control system is able to reduce the angular velocity in two of the three axes very quickly. However it takes some orbits to reduce the angular velocity in the pitch axis. Nevertheless the results show that it is feasible to implement this 3 axis control system together with a B-dot control law.

As will be discussed in the next chapter, a different choice of the control matrices S, Q and R will result in a different result. In this case, a possible choice would be to put more effort on reducing the angular velocity and no effort on the angles until the angular velocity reaches the target angular velocity. Then switch the control matrices for a fine pointing attitude controller.

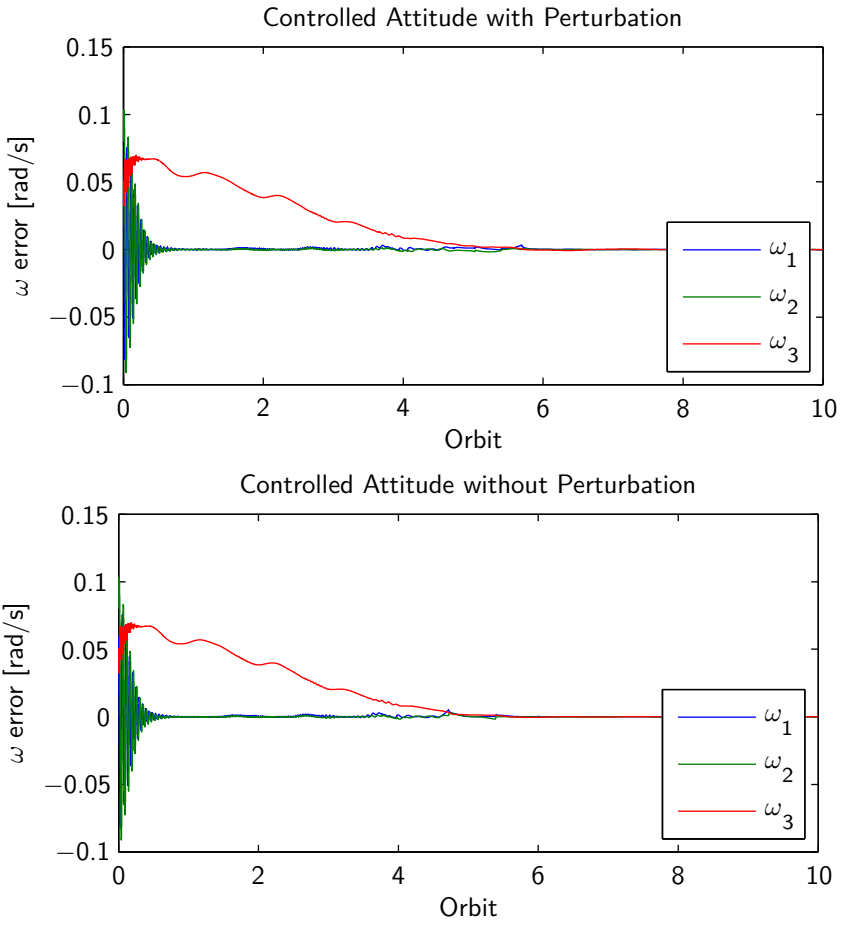

Figure 4.12: Angular velocity error

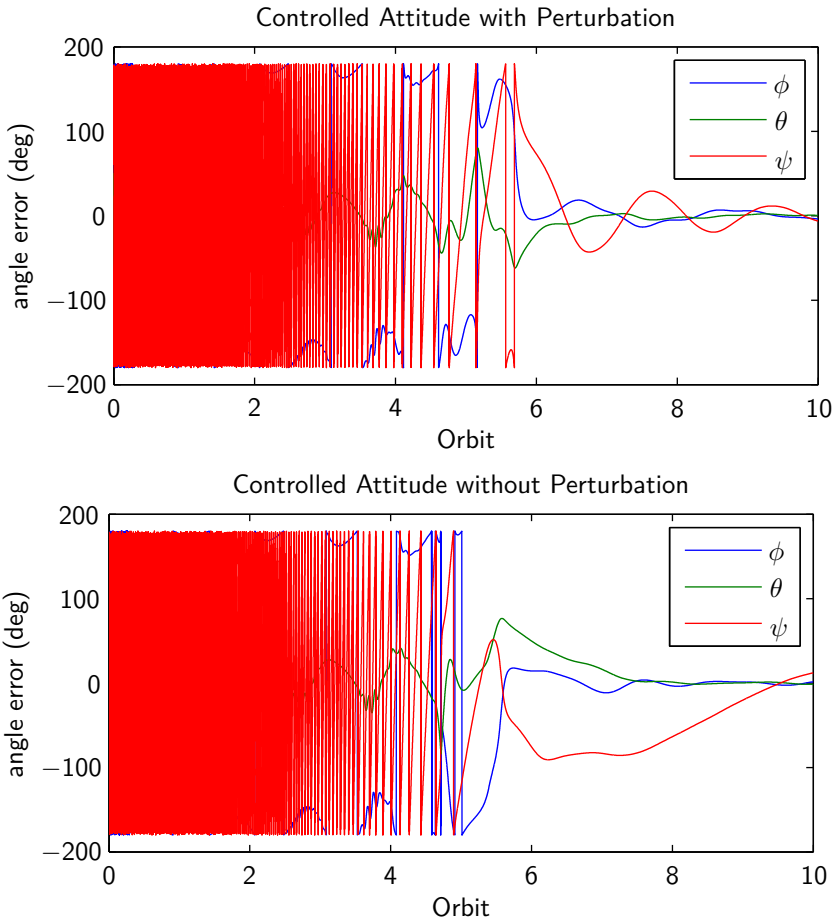

Figure 4.13: Angle error

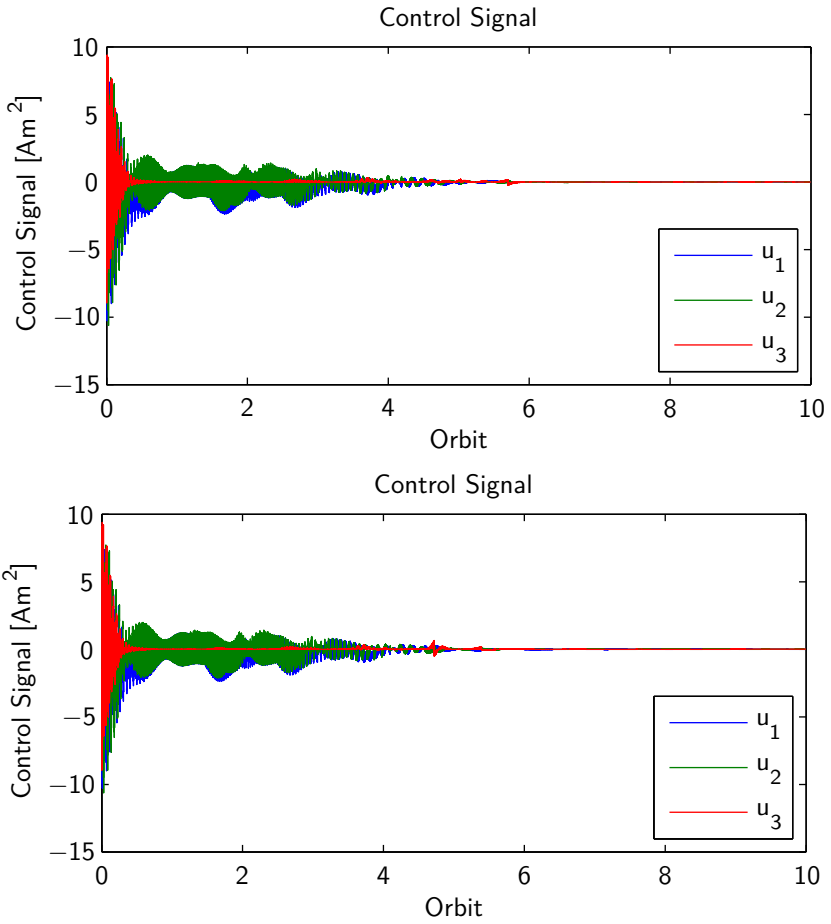

Figure 4.14: Envelope of the Control Signal

Comparing these results with those obtained with small initial conditions, several conclusions can be extracted. First, the control system takes more time to control one axis than the others in both situations. The cause has been explained previously, it is due to the small projection of the available Earth magnetic field along the orbital plane of a 15 degrees orbit. Second, the control action almost reached the limits of the magnetorquers described before, with a peak value of about $10Am^2$. Finally, these results also suggest that the control system will also be able to recover the control of the satellite under a very large unexpected perturbation in attitude.

4.3 Feasibility analysis

The results presented so far show a good performance for a certain orbit and several initial conditions. A set of simulations have been carried out in order to test the control system for several orbital conditions. The initial conditions on angular velocity and error angles are those used in the small initial conditions subset, represented in equation 4.5. Those conditions are zero error for angular velocity and an error in the target nadir pointing attitude of 2 degrees in roll, 1 degree in yaw and 0 degrees in pitch, the axis of the nominal angular velocity. The orbit altitude is 500 km above mean sea level.

Two performance index have been defined to evaluate the behavior of the satellite for the available orbits and present the results.

The first index takes into account the *control time*, which is defined as the time that any component of the quaternion vector takes in order to be less than 0.005; it means $|q_i| \leq 0.005$ (see Figure 4.15).

The second index is intended to measure the *effectiveness of the control*. Therefore, the mean value of the quaternion error vector during the 10th orbit is chosen.

The numerical results are summarized in tables 4.1 and 4.2, where the best values are in boldface. These results show that the control system works for a wide variety of orbits and that a better performance

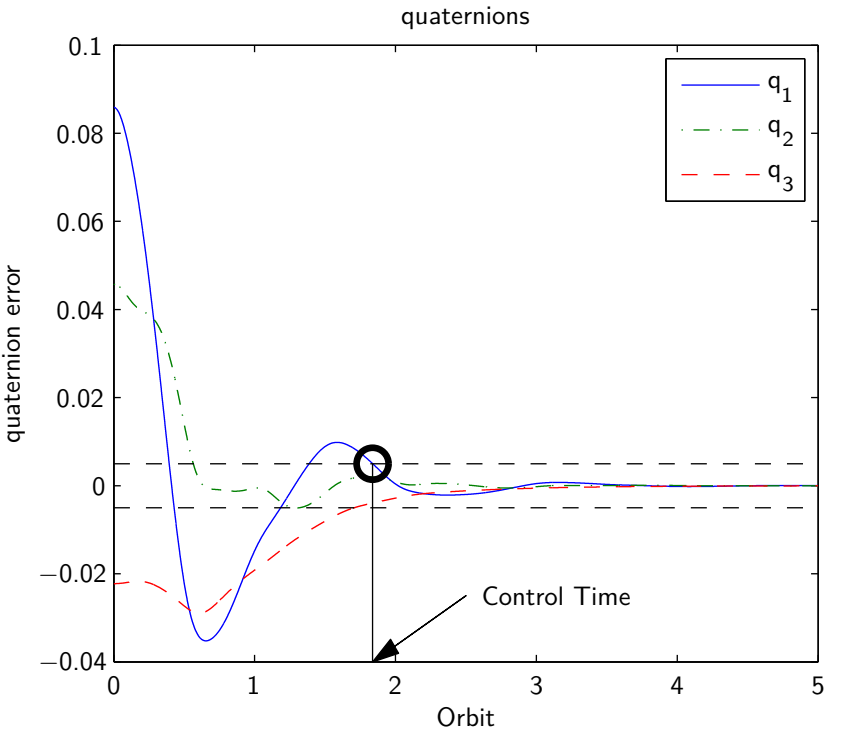

Figure 4.15: Control Time Definition

RAAN incl.	0	45	90	135	180	225	270	315	360
	Quaternion vector mean value [$\cdot 10^{-7}$]								
30 [$\cdot 10^{-3}$]	0,08	0,08	0,30	0,46	0,24	0,31	0,12	0,07	0,08
45 [$\cdot 10^{-5}$]	0,04	0,22	0,91	1,48	0,66	0,10	0,02	0,01	0,04
60	0,03	0,07	0,07	0,15	0,21	0,09	0,03	**0,01**	0,03
75	0,09	0,04	0,02	0,02	0,03	0,06	0,10	0,12	0,09
90	0,15	0,15	0,15	0,13	0,11	0,11	0,12	0,14	0,15

Table 4.1: Quaternion vector mean value, orbit height = 500 km

RAAN incl.	0	45	90	135	180	225	270	315	360
	Time [orbits]								
30	4,43	5,55	6,11	5,62	4,15	2,03	2,01	2,17	4,43
45	2,02	2,16	3,46	1,91	1,77	1,7	1,71	1,83	2,02
60	1,7	1,77	1,72	1,62	1,53	1,49	1,51	1,58	1,7
75	1,49	1,53	1,5	1,41	1,3	1,27	1,34	1,42	1,49
90	1,32	1,35	1,27	1,05	1,03	**1,02**	1,05	1,2	1,32

Table 4.2: Control Time, orbit height = 500 km

is achieved with high inclination orbits. Orbits with higher inclinations allow the satellite to move in a higher varying magnetic field than orbits with inclinations closer to Earth Magnetic equator. The effect of orbit inclination can be shown in figures 4.16 and 4.17, where an orbit of 15 degrees and 75 degrees respectively are plotted.

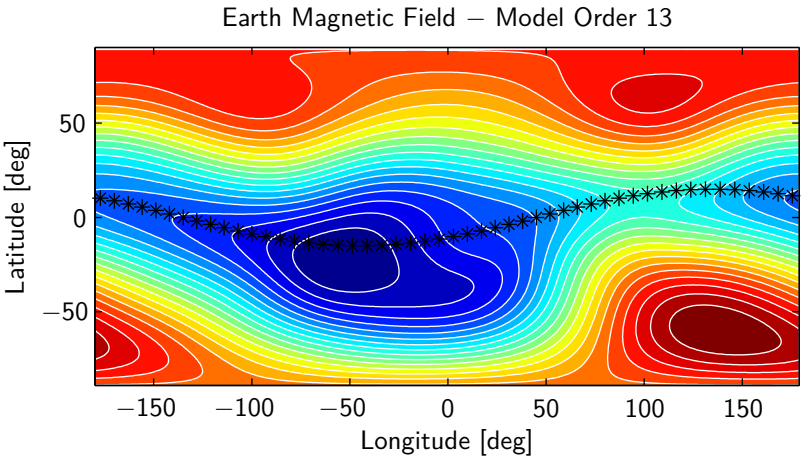

Figure 4.16: 15 degrees inclination orbit path and magnetic field

4.4 Conclusions of this chapter

Several Simulations have been carried out in order to test the control system. In section 4.1, a simulation of the system is analyzed. Along this simulation, the whole simulation environment and how the ASRE

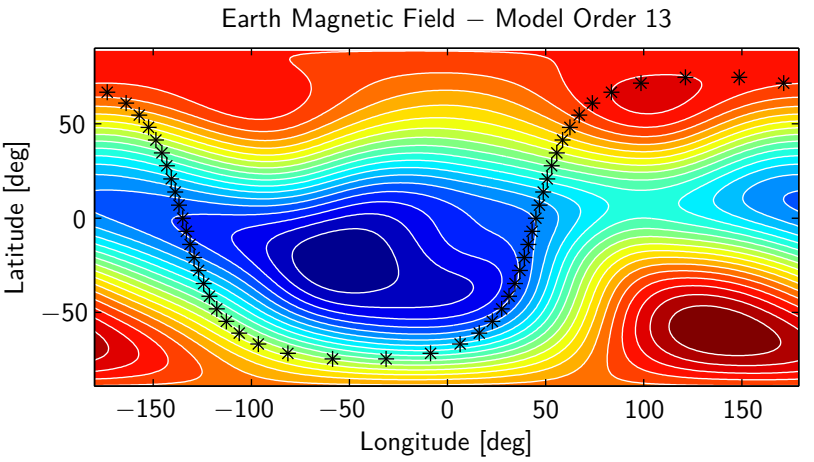

Figure 4.17: 75 degrees inclination orbit path and magnetic field

technique can be applied to attitude control is explained.

Then in section 4.2, the control system is checked under perturbations and model uncertainties for a certain orbit and initial conditions. It is shown that the control actions are well within the limits of the actuators for a satellite with similar inertia moments as the one under test. Furthermore the control strategy is able to control the satellite in case of large angular rates such as the ones that will remain after a detumbling phase using the well known Bdot algorithm.

Finally, in section 4.3, a bench of simulations are carried out in order to establish a feasibility analysis. The results show that the control system works for a wide variety of orbits and that a better performance is achieved with high inclination orbits.

5

Conclusions

In this work, a new algorithm for magnetic satellite attitude control system design is presented. In this method, only magnetic actuators are needed and three axis pointing accuracy is achieved using a non linear technique called *Approximating Sequence of Riccati Equations (ASRE)*. This technique is based on transforming the nonlinear control problem into an equivalent time variant problem with the introduction of the iterative sequence corresponding to the system dynamics and another iterative sequence corresponding to the cost function to be minimized. The new problem can be solved as a sequence of two point boundary value problems using the costate transformation as a soft Constrained Problem.

ASRE technique can solve the control problem for a given horizon time. However, it is not efficient at all to solve the problem for a

whole orbit, because the simulated state will not match the real state due to perturbation or model uncertainties. Therefore, a time span is introduced. Then, the control will be calculated in every time-span period.

The control system has been intensively proven for a wide variety of orbits and initial conditions. Model uncertainties and perturbations have been also taken into account. The results show that the control system works for a wide variety of orbits and that a better performance is achieved with high inclination orbits. Furthermore the control strategy is able to control the satellite in case of large angular rates such as the ones that will remain after a detumbling phase using the well known Bdot algorithm.

It is also shown that the control actions are well within the limits of the actuators for a satellite with similar inertia moments as the one under test. However the performances can be tailored to the available control power.

The contents in chapter 3 and 4 represent an improvement to the state of the art for three axis magnetic satellite attitude control. Only a few nonlinear techniques have been used in attitude control problems and none of them have been reported to fully control a magnetically actuated spacecraft in three axis without any other stabilization technique or using any other type of actuator.

6

Conclusiones

En este trabajo se presenta un nuevo algoritmo para un sistema de control magnético de orientación de satélites. La ventaja de este método de control sobre otros es que sólo se necesitan actuadores magnéticos. Además se consigue el apuntamiento de los tres ejes de libertad utilizando una técnica de control no lineal llamada *Approximating Sequence of Riccati Equations (ASRE)*. Esta técnica está basada en transformar el problema de control no lineal en un problema equivalente de tiempo variante mediante dos secuencias iterativas, una correspondiente a la dinámica del sistema y otra correspondiente a la función de coste que debe ser minimizada. El nuevo problema puede ser resuelto como una secuencia de problemas *Two points boundary value problems (TPBVP)* usando la transformación de coestado y resolviendo el problema como un *Soft Constrained Problem (SCP)*.

La técnica ASRE puede resolver el problema de control para un horizonte de tiempo dado. Sin embargo, no es eficiente resolver el problema de control para una órbita completa, ya que la propagación del estado simulado puede no reflejar la evolución del estado real debido a perturbaciones y discrepancias entre el modelo y la realidad. Por todo ello, se introduce un parámetro llamado *Time Span*. Entonces, el control será calculado in cada periodo de tiempo marcado por *time span*.

El sistema de control se ha probado intensamente para una gran variedad de órbitas y condiciones iniciales. También se han tenido en cuenta las perturbaciones y los errores de modelado. Los resultados demuestran que el sistema de control funciona para una gran variedad de órbitas, pero se consiguen los mejores resultados para órbitas de alta inclinación. Además, también se ha probado la estrategia de control para condiciones de velocidad angular similares a las que existirían después de una fase de *detumbling* utilizando el algoritmo *Bdot*.

También se demuestra que las acciones de control están dentro de los límites de funcionamiento de los actuadores electromagnéticos típicos para un satélite de las propiedades de inercia del que se ha elegido para las pruebas. No obstante, el funcionamiento puede ser personalizado según la potencia de control disponible.

El contenido de los capítulos 3 y 4 presenta una mejora en el estado del arte del control magnético en tres ejes de la orientación de un satélite. Sólo se han explorado unas pocas técnicas de control no lineal para resolver el problema de control magnético de la orientación, y ninguna de ellas han conseguido controlar totalmente un satélite con actuadores electromagnéticos en tres ejes sin utilizar alguna otra técnica de estabilización o usando otro tipo de actuadores.

7

Open Research Topics

Every research work helps to understand or provides solution to a known [or unknown] problem. Furthermore it opens new questions or topics which can be investigated in more detail. In this chapter, the open topics which might be considered in the future are discussed.

The first one is the modeling of the magnetic field. Although the control system presented in this work is able to control the satellite in every situation that has been tested, better results might be obtained if the full model of the magnetic field is introduced in the system model instead of the dipole model. This improvement will change the matrix B in equation 3.41, where β_{pi} should be calculated using the full model introduced in section 3.3. The contributions of a better modeling of the magnetic field would be higher in lower orbits and near the anomalies of the magnetic field, where the higher order terms

of the model become more dominant.

The factorization proposed in section 3.4 is not unique for the same system. Therefore another factorization which might contribute to the performance of the whole system could also be proposed.

ASRE related design issues for the problem considered in this work are still open. The optimization of the time span and the optimization of the control matrices Q, S an R should be studied for every case and orbit. For instance, taking the case in section 4.1 and changing matrix $R = I_3/2$, another performance of the system is achieved. The results for this case are shown in figures 7.1 to 7.3. The error on the scalar quaternion part and the angular velocity with different values of the time span is also plotted on figures 7.4 and 7.5.

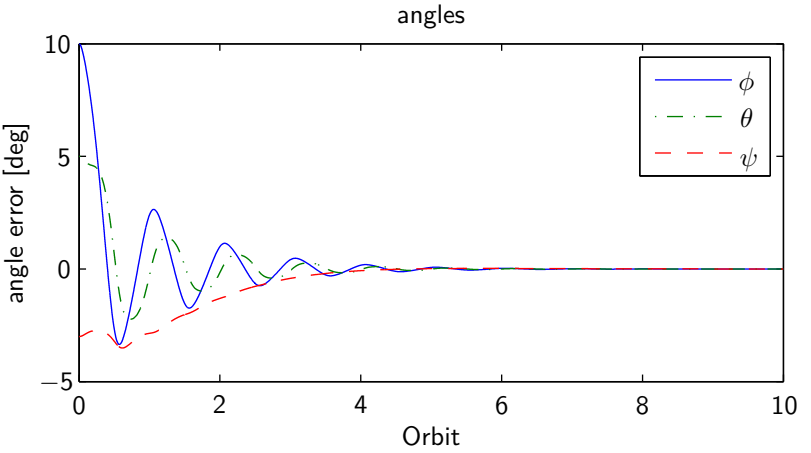

Figure 7.1: Angle error for R=0.5I

A more mechanical method for fine tuning of these parameters could be outlined. Another important property of the control algorithms is the study of stability regions or regions of attraction. In this work, a method based on a bench of simulation is presented in section 4.3. A more formal method needs to be formulated for stability analysis of this controller. A good starting point is the work by Banks [83].

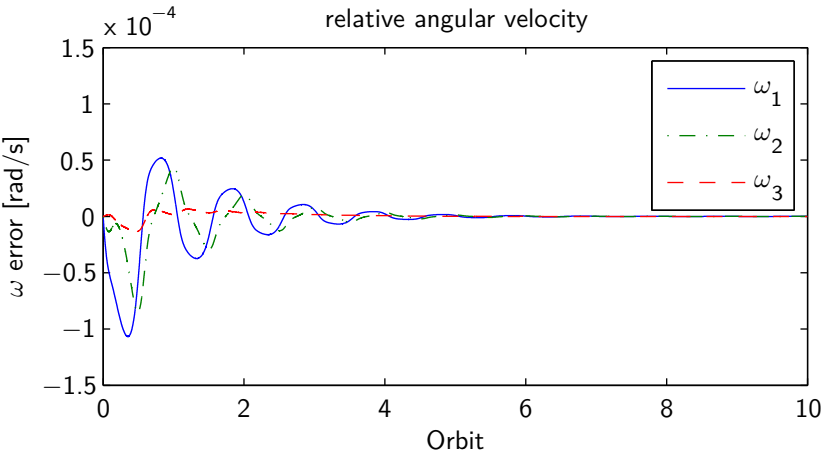

Figure 7.2: Angular velocity error for R=0.5I

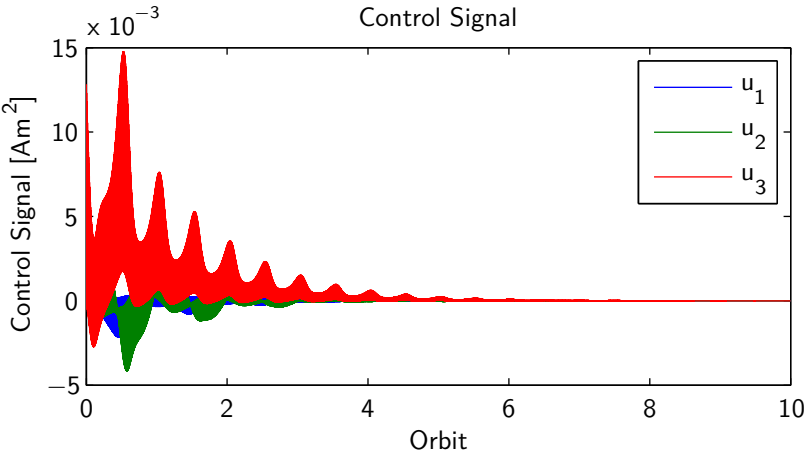

Figure 7.3: Control Signal for R=0.5I

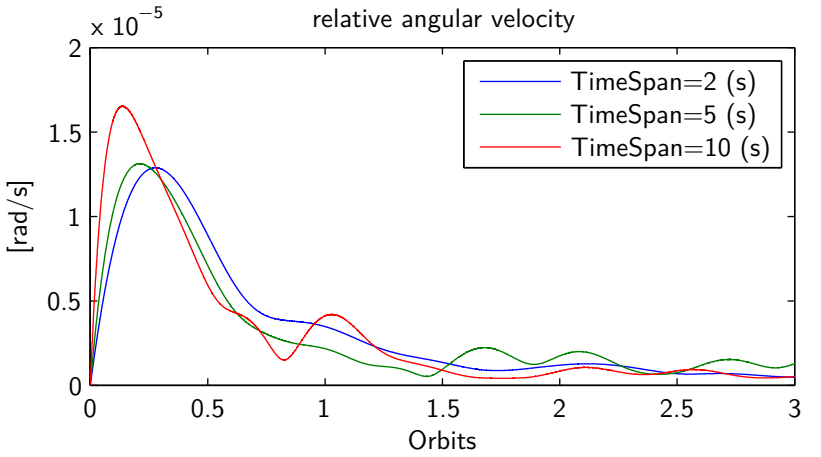

Figure 7.4: Quaternion error with different time spans

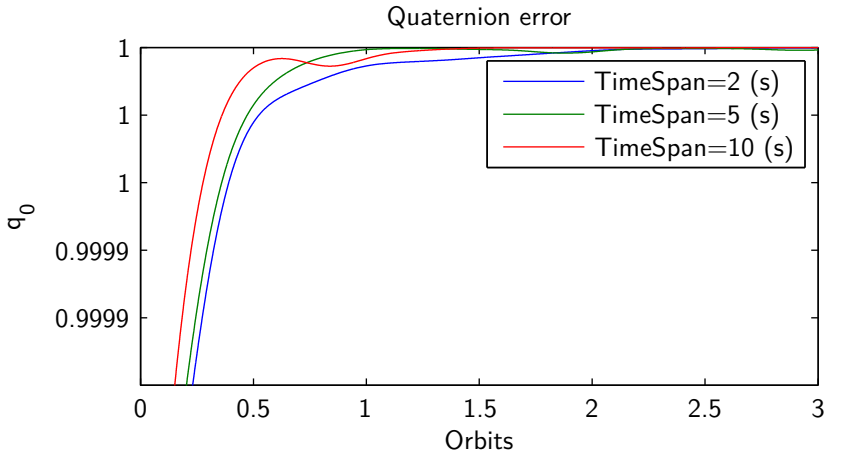

Figure 7.5: Angular velocity error with different time spans

Another very important issue is convergence time of the ASRE. Reducing the time span also reduces the convergence time for a given hardware setup. However, reducing the time span also reduces the time period of the calculated control, thus the algorithm should be rerun at a higher frequency. If the algorithm is to be implemented on board a given hardware, testing of the time the hardware takes to solve the ASRE problem should be undertaken.

All the algorithms should be tested on ground before launching. Special facilities are needed to test a magnetic attitude control system. A good review of satellite attitude testing facilities is presented in [87]. The facilities designed so far use 6 Helmholtz coils, two per axis, for the generation of a constant magnetic field in the region of interest located in the geometrical center of the coils. An air bearing table is situated in the center of the facility in order to provide torque free motion in 3 axis with restrictions in pitch and roll. Therefore, the satellite can be placed in the middle of the facility on the air bearing platform and the control attitude control system can be tested [88] . In order to simulate the magnetic field, a measure of the field present in the room is taken. Then the Helmholtz coils generate the desired magnetic field plus the appropriate component to cancel the magnetic field previously measured [89]. However, there are still open issues as how to compensate efficiently in closed loop the magnetic field and reach field levels in the order of magnitude as the magnetic field in a high orbit.

Finally, other applications of active magnetic attitude control can be explored in several fields other than aerospace. For instance, in [90] a study of magnetic navigation system design for microbots in biomedical applications is discussed.

Bibliography

[1] P.W. Fortescue, J. Stark, and G. Swinerd. *Spacecraft systems engineering*. J. Wiley, 2003. ISBN: 9780470851029. URL: http://books.google.es/books?id=_KCNcxYPUZgC.

[2] E.D. Scott. "Control moment gyro gravity stabilization". In: *Guidance and Control Conference*. AIAA, 1963.

[3] Michele Carpenter. "Power-Optimal Steering of a Space Robotic System Driven by Control-Moment Gyroscopes". In: *Guidance, Navigation, and Control and Co-located Conferences*. American Institute of Aeronautics and Astronautics, Aug. 2008, pp. –. DOI: 10.2514/6.2008-7270. URL: http://dx.doi.org/10.2514/6.2008-7270.

[4] Hyungjoo Yoon and Panagiotis Tsiotras. "Spacecraft Line-of-Sight Control Using a Single Variable-Speed Control Moment Gyro". In: *Journal of Guidance, Control, and Dynamics* 29.6 (Nov. 2006), pp. 1295–1308. ISSN: 0731-5090. DOI: 10.2514/1.18777. URL: http://dx.doi.org/10.2514/1.18777.

[5] Laura L. Jones, Rodrigo A. Zeledon, and Mason A. Peck. "Generalized Framework for Linearly Constrained Control Moment Gyro Steering". In: *Journal of Guidance, Control, and Dynamics* 35.4 (July 2012), pp. 1094–1103. ISSN: 0731-5090. DOI: 10.2514/1.56207. URL: http://dx.doi.org/10.2514/1.56207.

[6] Kohei Takada, Hirohisa Kojima, and Naoki Matsuda. "Control Moment Gyro Singularity-Avoidance Steering Control Based on Singular-Surface Cost Function". In: *Journal of Guidance, Control, and Dynamics* 33.5 (Sept. 2010), pp. 1442–1450. ISSN: 0731-5090. DOI: 10.2514/1.48381. URL: http://dx.doi.org/10.2514/1.48381.

[7] James R. Wertz. *Spacecraft Attitude Determination and Control*. Kluwer Academic Publishers, 1978.

[8] G. A. Beals et al. "Hubble Space Telescope precision pointing control system". In: *Journal of Guidance, Control, and Dynamics* 11.2 (Mar. 1988), pp. 119–123. ISSN: 0731-5090. DOI: 10.2514/3.20280. URL: http://dx.doi.org/10.2514/3.20280.

[9] W.J. Larson and J.R. Wertz. *Space mission analysis and design*. Space technology library. Microcosm, 1992. ISBN: 9780792319986.

[10] F. Landis Markley et al. "Maximum Torque and Momentum Envelopes for Reaction Wheel Arrays". In: *Journal of Guidance, Control, and Dynamics* 33.5 (Sept. 2010), pp. 1606–1614. ISSN: 0731-5090. DOI: 10.2514/1.47235. URL: http://dx.doi.org/10.2514/1.47235.

[11] D. Desiderio et al. "Magnetic momentum management for a geostationary satellite platform". In: *Control Theory & Applications, IET* 3.10 (2009), pp. 1370–1382. ISSN: 1751-8644. DOI: http://dx.doi.org/10.1049/iet-cta.2008.0327.

[12] M.J.L. Turner. *Rocket And Spacecraft Propulsion: Principles, Practice And New Developments*. Astronautical engineering. Springer London, Limited, 2005. ISBN: 9783540221906.

[13] Boucher R. "Electrical propulsion for control of stationary satellites". In: *International Electric Propulsion Conference*. American Institute of Aeronautics and Astronautics, Mar. 1963, pp. –. DOI: 10.2514/6.1963-9. URL: http://dx.doi.org/10.2514/6.1963-9.

[14] Giovanni Matticari et al. “Cold Gas Micro Propulsion Prototype for Very Fine Spacecraft Attitude/Position Control”. In: *Joint Propulsion Conferences*. American Institute of Aeronautics and Astronautics, July 2006, pp. –. DOI: 10.2514/6.2006-4872. URL: http://dx.doi.org/10.2514/6.2006-4872.

[15] V. Haloulakos. “Thrust and impulse requirements for jet attitude-control systems”. In: *Meeting Paper Archive*. American Institute of Aeronautics and Astronautics, June 1963, pp. –. DOI: 10.2514/6.1963-237. URL: http://dx.doi.org/10.2514/6.1963-237.

[16] P R. Dahl, L. K. Herman, and G. T Aldrich. “Limit Cycles In Reaction Jet Attitude Control Systems Subject To External Torques”. In: *Guidance And Control*. American Institute of Aeronautics and Astronautics, 1962. DOI: 10.2514/5.9781600864827.0599.0627. URL: http://dx.doi.org/10.2514/5.9781600864827.0599.0627.

[17] D. Fosth and W. Mitchell. “Lunar Orbiter Attitude Control System”. In: *Meeting Paper Archive*. American Institute of Aeronautics and Astronautics, Aug. 1967, pp. –. DOI: 10.2514/6.1967-533. URL: http://dx.doi.org/10.2514/6.1967-533.

[18] Allan Lee and Gene Hanover. “Cassini Spacecraft Attitude Control System Flight Performance”. In: *Guidance, Navigation, and Control and Co-located Conferences*. American Institute of Aeronautics and Astronautics, Aug. 2005, pp. –. DOI: 10.2514/6.2005-6269. URL: http://dx.doi.org/10.2514/6.2005-6269.

[19] R. Prigge, H. Klotz, and H. Strauch. “Spacecraft attitude control using magnetic torquers and gas jets”. In: *Proceedings of the First ESA International Conference of Spacecraft Guidance, Navigation, and Control Systems*. Vol. 323. 1991, pp. 491 –496.

[20] Dan M. Goebel and Ira Katz. *Fundamentals of Electric Propulsion: Ion and Hall Thrusters*. JPL Space Science and Technology Series. Jet Propulsion Laboratoy, Mar. 2008.

[21] E. Y. Choueiri. "A Critical History of Electric Propulsion: The First 50 Years (1906-1956)". In: *Journal of Propulsion and Power* 20.2 (Mar. 2004), pp. 193–203. ISSN: 0748-4658. DOI: 10.2514/1.9245. URL: http://dx.doi.org/10.2514/1.9245.

[22] R. Jahn and W. Mickelsen. "Status of electric propulsion". In: *Joint Propulsion Conferences*. American Institute of Aeronautics and Astronautics, June 1969, pp. –. DOI: 10.2514/6.1969-497. URL: http://dx.doi.org/10.2514/6.1969-497.

[23] James S. Sovey, Vincent K. Rawlin, and Michael J. Patterson. "Ion Propulsion Development Projects in U.S.: Space Electric Rocket Test 1 to Deep Space 1". In: *Journal of Propulsion and Power* 17.3 (May 2001), pp. 517–526. ISSN: 0748-4658. DOI: 10.2514/2.5806. URL: http://dx.doi.org/10.2514/2.5806.

[24] Anita Sengupta et al. "Deep Space 1 Flight Spare Ion Thruster 30,000-Hour Life Test". In: *Journal of Propulsion and Power* 25.1 (Jan. 2009), pp. 105–117. ISSN: 0748-4658. DOI: 10.2514/1.36549. URL: http://dx.doi.org/10.2514/1.36549.

[25] Giorgio Mingotti, Francesco Topputo, and Franco Bernelli-Zazzera. "Hybrid Propulsion Transfer to the Moon". In: *First IAA Conference on Dynamics and Control of Space Systems 2012*. Ed. by Anna D. Guerman, Peter M. Bainum, and Jean-Michel Contant. Advances in the Astronautical Sciences AAS 12-214. American Astronautical Society - Univelt, Mar. 2012.

[26] Rainer Killinger et al. "ARTEMIS: Ion Propulsion - Satellite Interactions". In: *Joint Propulsion Conferences*. American Institute of Aeronautics and Astronautics, July 2005, pp. –. DOI: 10.2514/6.2005-3670. URL: http://dx.doi.org/10.2514/6.2005-3670.

[27] Christopher D. Rayburn, Mark E. Campbell, and A. Thomas Mattick. "Pulsed Plasma Thruster System for Microsatellites". In: *Journal of Spacecraft and Rockets* 42.1 (Jan. 2005), pp. 161–

170. ISSN: 0022-4650. DOI: 10.2514/1.15422. URL: http://dx.doi.org/10.2514/1.15422.

[28] Michael Patterson. "Next-Generation Electric Propulsion Thrusters". In: *Joint Propulsion Conferences*. American Institute of Aeronautics and Astronautics, July 2011, pp. –. DOI: 10.2514/6.2011-5812. URL: http://dx.doi.org/10.2514/6.2011-5812.

[29] Marc G. Millis and Eric W. Davis. *Frontiers of Propulsion Science*. American Institute of Aeronautics and Astronautics, 2009.

[30] Hector H. Brito and Sergio A. Elaskar. "Direct Experimental Evidence of Electromagnetic Inertia Manipulation Thrusting". In: *Journal of Propulsion and Power* 23.2 (Aug. 2007), pp. 487–494. ISSN: 0748-4658. DOI: 10.2514/1.18897. URL: http://dx.doi.org/10.2514/1.18897.

[31] Hector Brito, Ricardo Marini, and Eugenio Galian. "Null Findings on Electromagnetic Inertia Thrusting Experiments Using a Torsion Pendulum". In: *Joint Propulsion Conferences*. American Institute of Aeronautics and Astronautics, Aug. 2009, pp. –. DOI: 10.2514/6.2009-5070. URL: http://dx.doi.org/10.2514/6.2009-5070.

[32] Ronald S. Maynard. *Fluidic momentum controller*. Oct. 1988.

[33] Theodore C. Iskenderian, Boris J. Lurie, and J. Alan Schier. *Fluid-loop reaction system*. June 1991.

[34] K.D. Kumar. "Satellite attitude stabilization using fluid rings". In: *Acta Mechanica* 208.1-2 (2009), pp. 117–131. ISSN: 0001-5970. DOI: 10.1007/s00707-008-0132-5. URL: http://dx.doi.org/10.1007/s00707-008-0132-5.

[35] Nona A. Nobari and Arun K. Misra. "Attitude Dynamics and Control of Satellites With Fluid Ring Actuators". In: *Journal of Guidance, Control, and Dynamics* 35.6 (Oct. 2012), pp. 1855–1864. ISSN: 0731-5090. DOI: 10.2514/1.54599. URL: http://dx.doi.org/10.2514/1.54599.

[36] M.J. Sidi. *Spacecraft Dynamics and Control: A Practical Engineering Approach*. Cambridge aerospace series. Cambridge University Press, 2000. ISBN: 9780521787802. URL: http://books.google.es/books?id=xQpZJMtDehQC.

[37] M. S. Hodgart and P. S. Wright. "Attitude determination, control and stabilization of UoSAT-2". In: *Electronic and Radio Engineers, Journal of the Institution of* 57.5 (1987), S151–S162. ISSN: 0267-1689. DOI: 10.1049/jiere.1987.0085.

[38] M.Yu. Ovchinnikov et al. "Nanosatellite REFLECTOR: Choice of parameters of the attitude control system". In: *Cosmic Research* 45.1 (2007), pp. 60–77. ISSN: 0010-9525. DOI: 10.1134/S0010952507010078. URL: http://dx.doi.org/10.1134/S0010952507010078.

[39] M. S. Hodgart. "Attitude control and dynamics of UOSAT angular motion". In: *Radio and Electronic Engineer* 52.8.9 (1982), pp. 379–384. ISSN: 0033-7722. DOI: 10.1049/ree.1982.0055.

[40] G.C. Weiffenbach. "The genesis of TRANSIT". In: *Aerospace and Electronic Systems, IEEE Transactions on* AES-22.4 (1986), pp. 474–481. ISSN: 0018-9251. DOI: 10.1109/TAES.1986.310791.

[41] H. D. Black. "Early development of Transit, the Navy navigation satellite system". In: *Journal of Guidance, Control, and Dynamics* 13.4 (July 1990), pp. 577–585. ISSN: 0731-5090. DOI: 10.2514/3.25373. URL: http://dx.doi.org/10.2514/3.25373.

[42] Robert E. Fischell. "Passive Magnetic Attitude Control for Earth Satellites". In: *Advances in the Astronautical Sciences* 11 (1963), pp. 147 –176.

[43] Michael Ovchinnikov et al. "Attitude control system for the first swedish nanosatellite MUNIN". In: *Acta Astronautica* 46 (2000), pp. 319–326. ISSN: 0094-5765. URL: http://www.sciencedirect.com/science/article/pii/S009457659900226X.

[44] M.Yu. Ovchinnikov and V.I. Penkov. "Passive Magnetic Attitude Control System for the Munin Nanosatellite". In: *Cosmic Research* 40.2 (2002), pp. 142–156. ISSN: 0010-9525. DOI: 10.1023/A:1015197303662. URL: http://dx.doi.org/10.1023/A%3A1015197303662.

[45] Fabio Santoni and Mauro Zelli. "Passive magnetic attitude stabilization of the UNISAT-4 microsatellite". In: *Acta Astronautica* 65 (2009), pp. 792–803. ISSN: 0094-5765. URL: http://www.sciencedirect.com/science/article/pii/S0094576509001568.

[46] S.O. Karpenko et al. "Attitude control system of the first Russian nanosatellite TNS-0 no. 1". In: *Cosmic Research* 48.6 (2010), pp. 517–525. ISSN: 0010-9525. DOI: 10.1134/S0010952510060043. URL: http://dx.doi.org/10.1134/S0010952510060043.

[47] Michael Ovchinnikov. "Attitude Dynamics of a Small-Sized Satellite Equipped with Hysteresis Damper". In: *Advances in the Astronautical Sciences Series*. Ed. by Anna D. Guerman, Peter M. Bainum, and Jean-Michel Contant. Vol. 145. 2012.

[48] John S. White, Fred H. Shigemoto, and Kent Bourquin. *Satellite Attitude Control Utilizing the Earth's Magnetic Field*. Tech. rep. Ames Research Center, Moffett Field, CA: NASA TN D-1068, 1961.

[49] A. Craig Stickler and K.T. Alfriend. "Elementary Magnetic Attitude Control System". In: *Journal of Spacecraft and Rockets* 13.5 (1976), pp. 282 –287.

[50] K. Raman and S. Rajaram. "Magnetic roll/yaw control of a momentum biased communication spacecraft using an observer approach and a servo compensator approach". In: *Guidance, Navigation, and Control and Co-located Conferences*. American Institute of Aeronautics and Astronautics, Aug. 1989, pp. –. DOI: 10.2514/6.1989-3478. URL: http://dx.doi.org/10.2514/6.1989-3478.

[51] Mark E. Pittelkau. "Optimal periodic control for spacecraft pointing and attitude determination". In: *Journal of Guidance, Control, and Dynamics* 16.6 (Nov. 1993), pp. 1078–1084. ISSN: 0731-5090. DOI: 10.2514/3.21130. URL: http://dx.doi.org/10.2514/3.21130.

[52] T. Prieto-Llanos and G. Fdez. de la Mora. "Spain's minisat attitude determination and control system (ADCS)". In: *2nd ESA International Conference on GNC*. 1994, pp. 51 –57.

[53] S. M. Wolfe, K. T. Alfriend, and B. S. Leonard. "A Magnetic Attitude Control System for Sun Pointing Satellites". In: *Astrodynamics Specialists Conference*. 1995.

[54] Fabio Santoni and Paolo Tortora. "Magnetic attitude determination and control of small spinning spacecraft". In: *Guidance, Navigation, and Control and Co-located Conferences*. American Institute of Aeronautics and Astronautics, Aug. 2000, pp. –. DOI: 10.2514/6.2000-4350. URL: http://dx.doi.org/10.2514/6.2000-4350.

[55] Fabrizio Giulietti, Alessandro A. Quarta, and Paolo Tortora. "Optimal Control Laws for Momentum-Wheel Desaturation Using Magnetorquers". In: *Journal of Guidance, Control, and Dynamics* 29.6 (Nov. 2006), pp. 1464–1468. ISSN: 0731-5090. DOI: 10.2514/1.23396. URL: http://arc.aiaa.org/doi/abs/10.2514/1.23396.

[56] M.Yu. Ovchinnikov, V.I. Pen'kov, and D.S. Roldugin. "Study of a bunch of three algorithms for magnetic control of attitude and spin rate of a spin-stabilized satellite". In: *Cosmic Research* 50.4 (2012), pp. 304–312. ISSN: 0010-9525. DOI: 10.1134/S0010952512040041. URL: http://dx.doi.org/10.1134/S0010952512040041.

[57] Giulio Avanzini, Emanuele L. de Angelis, and Fabrizio Giulietti. "Single-axis Pointin of a Magnetically Actuated Spacecraft". In: *First IAA Conference on Dynamics and Control of Space Sys-*

tems 2012. Ed. by Anna D. Guerman, Peter M. Bainum, and Jean-Michel Contant. Advances in the Astronautical Sciences AAS 12-317. American Astronautical Society - Univelt, Mar. 2012. ISBN: 978-0-87703-588-6.

[58] G. Avanzini, E.L. de Angelis, and F. Giulietti. "Spin-axis pointing of a magnetically actuated spacecraft". In: *Acta Astronautica* (2013). ISSN: 0094-5765. DOI: 10.1016/j.actaastro.2012.10.035. URL: http://www.sciencedirect.com/science/article/pii/S0094576512004249.

[59] F. Martel, P.K. Pal, and M. Psiaki. "Active Magnetic Control System for Gravity Gradient Stabilized Spacecraft". In: *Proceedings of 2nd Annual AIAA/USU Conference on Small Satellites*. 1988.

[60] K Austin, A McGhee, and SF Asokanthan. "Attitude Control and Stabilization for the AUSTRALIS 1 Micro-satellite Project". In: *National Space Engineering Symposium (8th : 1993 : University of Queensland)*. 1993, pp. 84–92.

[61] Willem H. Steyn. "Comparison of low-earth-orbit satellite attitude controllers submitted to controllability constraints". In: *Journal of Guidance, Control, and Dynamics* 17.4 (July 1994), pp. 795–804. ISSN: 0731-5090. DOI: 10.2514/3.21269. URL: http://dx.doi.org/10.2514/3.21269.

[62] M. Lovera and A. Astolfi. "Global magnetic attitude control of spacecraft in the presence of gravity gradient". In: *Aerospace and Electronic Systems, IEEE Transactions on* 42.3 (July 2006), pp. 796–805. ISSN: 0018-9251. DOI: 10.1109/TAES.2006.248214.

[63] Thomas W. Flatley et al. "A B-Dot Acquisition Controller for the RADARSAT Spacecraft". In: *NASA Conference Publication*. NASA. 1997, pp. 79–90.

[64] M. Yu. Ovchinnikov et al. "Investigation of the Effectiveness of an Algorithm of Active Magnetic Damping". In: *Cosmic Research* 50.2 (2012), pp. 170 –176. DOI: 10.1134/S0010952512010078.

[65] Giulio Avanzini and Fabrizio Giulietti. "Magnetic Detumbling of a Rigid Spacecraft". In: *Journal of Guidance, Control, and Dynamics* 35.4 (July 2012), pp. 1326–1334. ISSN: 0731-5090. DOI: 10.2514/1.53074. URL: http://dx.doi.org/10.2514/1.53074.

[66] Enrico Silani and Marco Lovera. "Magnetic spacecraft attitude control: a survey and some new results". In: *Control Engineering Practice* 13.3 (2005). Aerospace {IFAC} 2002, pp. 357 –371. ISSN: 0967-0661. DOI: 10.1016/j.conengprac.2003.12.017. URL: http://www.sciencedirect.com/science/article/pii/S0967066103002922.

[67] Rafal Wisniewski. "Satellite Attitude Control using Only Electromagnetic Actuation". PhdThesis. Fredrik Bajers Vej 7, DK-9220 Aalborg, Denmark.: Aalborg University, Dec. 1996.

[68] Rafal Wisniewski. "Linear Time-Varying Approach to Satellite Attitude Control Using Only Electromagnetic Actuation". In: *Journal of Guidance, Control, and Dynamics* 23.4 (July 2000), pp. 640–647. ISSN: 0731-5090. DOI: 10.2514/2.4609. URL: http://dx.doi.org/10.2514/2.4609.

[69] Rafal Wisniewski and Jakob Stoustrup. "Periodic H2 Synthesis for Spacecraft Attitude Control with Magnetorquers". In: *Journal of Guidance, Control, and Dynamics* 27.5 (Sept. 2004), pp. 874–881. ISSN: 0731-5090. DOI: 10.2514/1.10457. URL: http://dx.doi.org/10.2514/1.10457.

[70] M. Lovera, E. De Marchi, and S. Bittanti. "Periodic attitude control techniques for small satellites with magnetic actuators". In: *Control Systems Technology, IEEE Transactions on* 10.1 (Jan. 2002), pp. 90–95. ISSN: 1063-6536. DOI: 10.1109/87.974341.

[71] M. Lovera and A. Astolfi. "Spacecraft attitude control using magnetic actuators". In: *Automatica* 40.8 (2004), pp. 1405 –1414. ISSN: 0005-1098. DOI: 10.1016/j.automatica.2004.02.022.

URL: http://www.sciencedirect.com/science/article/pii/S0005109804000767.

[72] M. Lovera and A. Astolfi. "Global Magnetic Attitude Control of Inertially Pointing Spacecraft". In: *Journal of Guidance, Control, and Dynamics* 28.5 (Sept. 2005), pp. 1065–1072. ISSN: 0731-5090. DOI: 10.2514/1.11844. URL: http://dx.doi.org/10.2514/1.11844.

[73] James Richard Forbes and Christopher J. Damaren. "Linear Time-Varying Passivity-Based Attitude Control Employing Magnetic and Mechanical Actuation". In: *Journal of Guidance, Control, and Dynamics* 34.5 (Sept. 2011), pp. 1363–1372. ISSN: 0731-5090. DOI: 10.2514/1.51899. URL: http://dx.doi.org/10.2514/1.51899.

[74] Mark L. Psiaki. "Magnetic Torquer Attitude Control via Asymptotic Periodic Linear Quadratic Regulation". In: *Journal of Guidance, Control, and Dynamics* 24.2 (Mar. 2001), pp. 386–394. ISSN: 0731-5090. DOI: 10.2514/2.4723. URL: http://dx.doi.org/10.2514/2.4723.

[75] Tiziano Pulecchi, M. Lovera, and A. Varga. "Optimal Discrete-Time Design of Three-Axis Magnetic Attitude Control Laws". In: *Control Systems Technology, IEEE Transactions on* 18.3 (2010), pp. 714–722. ISSN: 1063-6536. DOI: 10.1109/TCST.2009.2024757.

[76] Vladimir A. Bushenkov, Michael Yu. Ovchinnikov, and Georgi V. Smirnov. "Attitude stabilization of a satellite by magnetic coils". In: *Acta Astronautica* 50.12 (2002), pp. 721 –728. ISSN: 0094-5765. DOI: 10.1016/S0094-5765(02)00011-5.

[77] D. Roldugin and P. Testani. "Active Magnetic Attitude Control System for Sun-pointing of a Spn Stabilized Satellite without Initial Detumbling". In: *First IAA Conference on Dynamics and Control of Space Systems 2012*. Ed. by Anna D. Guerman, Peter M. Bainum, and Jean-Michel Contant. Advances in the Astro-

nautical Sciences AAS 12-345. American Astronautical Society - Univelt, Mar. 2012. ISBN: 978-0-87703-588-6.

[78] International Association of Geomagnetism and Aeronomy et al. "International Geomagnetic Reference Field: the eleventh generation". In: *Geophysical Journal International* 183.3 (2010), pp. 1216–1230. ISSN: 1365-246X. DOI: 10.1111/j.1365-246X.2010.04804.x. URL: http://dx.doi.org/10.1111/j.1365-246X.2010.04804.x.

[79] Yaguang Yang. "Quaternion based model for momentum biased nadir pointing spacecraft". In: *Aerospace Science and Technology* 14 (2010), pp. 199–202.

[80] Tayfun Çimen. "State-Dependent Riccati Equation (SDRE) Control: A Survey". In: *Proceedings of the 17th World Congress of the IFAC*. The International Federation of Automatic Control, July 2008, pp. 3761 –3775.

[81] James R. Cloutier and Curtis P. Mracek. "Control Designs for the Nonlinear Benchmark Problem via the State-Dependent Riccati Equation Method". In: *International Journal of Robust Nonlinear Control* (Aug. 1998), pp. 401–433.

[82] Tayfun Çimen. "Systematic and effective design of nonlinear feedback controllers via the state-dependent Riccati equation (SDRE) method". In: *Annual Reviews in Control* 34.1 (2010), pp. 32 –51. ISSN: 1367-5788. DOI: 10.1016/j.arcontrol.2010.03.001. URL: http://www.sciencedirect.com/science/article/pii/S1367578810000052.

[83] Tayfun Çimen and Stephen P. Banks. "Global optimal feedback control for general nonlinear systems with nonquadratic performance criteria". In: *Systems and Control Letters* 53.5 (2004), pp. 327 –346. ISSN: 0167-6911. DOI: 10.1016/j.sysconle.2004.05.008. URL: http://www.sciencedirect.com/science/article/pii/S0167691104000817.

[84] Tayfun Çimen and Stephen P. Banks. "Nonlinear optimal tracking control with application to super-tankers for autopilot design". In: *Automatica* 40.11 (2004), pp. 1845 –1863. ISSN: 0005-1098. DOI: 10.1016/j.automatica.2004.05.015. URL: http://www.sciencedirect.com/science/article/pii/S0005109804001724.

[85] F. Topputo and F. Bernelli-Zazzera. "Optimal Low-Thrust Station Keeping of Geostationary Satellites". In: *3rd CEAS Air&Space Conference and XXI Congresso Nazionale AIDAA*. Oct. 2011, pp. 1917 –1925.

[86] Francesco Topputo and Franco Bernelli-Zazzera. "A Method to solve Nonlinear Optimal Control Problems in Astrodynamics". In: *First IAA Conference on Dynamics and Control of Space Systems 2012*. Ed. by Anna D. Guerman, Peter M. Bainum, and Jean-Michel Contant. Advances in the Astronautical Sciences AAS 12-398. American Astronautical Society - Univelt, Mar. 2012. ISBN: 978-0-87703-588-6.

[87] Jana L. Schwartz, Mason A. Peck, and Christopher D. Hall. "Historical Review of Air-Bearing Spacecraft Simulators". In: *Journal of Guidance, Control, and Dynamics* 26.4 (July 2003), pp. 513–522. ISSN: 0731-5090. DOI: 10.2514/2.5085. URL: http://dx.doi.org/10.2514/2.5085.

[88] D.S. Ivanov et al. "Testing of attitude control algorithms for microsatellite ChibisMat laboratory facility". In: *Journal of Computer and Systems Sciences International* 51.1 (2012), pp. 106–125. ISSN: 1064-2307. DOI: 10.1134/S1064230711060104. URL: http://dx.doi.org/10.1134/S1064230711060104.

[89] Christian Raschke, Stephan Roemer, and Karsten Grossekatthoefer. *Test bed for verification of attitude control system*. URL: http://www.astrofein.com/2728/dwnld/admin/Paper_TestBed.pdf.

[90] Quanliang Cao et al. "Analysis and Optimal Design of Magnetic Navigation System Using Helmholtz and Maxwell Coils". In:

Applied Superconductivity, IEEE Transactions on 22.3 (2012), pp. 4401504–4401504. ISSN: 1051-8223. DOI: 10.1109/TASC.2011.2174583.

[91] E. Bekir. *Introduction to modern navigation systems*. World Scientific, 2007. ISBN: 9789812707659. URL: http://books.google.es/books?id=RtUZAQAAIAAJ.

[92] Hamilton. *Elements of Quaternions*. London: Longmans, Green and Co., 1866.

A

Cross Product and Skew Symmetric Matrix

Modeling real life dynamics and kinematics using algebra usually implies the use of the well known vector cross product. Given two vectors $\vec{u} = [u_1, u_2, u_3]^T$ and $\vec{v} = [v_1, v_2, v_3]^T$, the cross product is denoted by $\vec{w} = \vec{u} \wedge \vec{v}$ and is defined by equation A.1.

$$\vec{w} = \vec{u} \wedge \vec{v} = \begin{bmatrix} u_2 v_3 - u_3 v_2 \\ u_3 v_1 - u_1 v_3 \\ u_1 v_2 - u_2 v_1 \end{bmatrix} \tag{A.1}$$

The result of the vector cross product of $\vec{u}$ and $\vec{v}$ is another vector $\vec{w}$ which direction is perpendicular to both $\vec{u}$ and $\vec{v}$. Thus, provided that the vector $\vec{k}$ is the unit vector perpendicular to both $\vec{u}$ and $\vec{v}$

given by the right hand rule, the cross product can be expressed by equation A.2.

$$\vec{w} = \vec{u} \wedge \vec{v} = |\vec{u}|\,|\vec{v}| \sin(\vec{u}, \vec{v})\vec{k} \tag{A.2}$$

Following the expression in equation A.2, it is straightforward to derive that $\vec{u} \wedge \vec{v} = -\vec{v} \wedge \vec{u}$.

A skew symmetric matrix B is a matrix with the property of $B' = -B$. The operator $S(\cdot)$ can be defined so that for a given vector $\vec{u}$, the skew symmetric vector in equation A.3 is derived.

$$S(\vec{u}) = \begin{bmatrix} 0 & -u_3 & u_2 \\ u_3 & 0 & -u_1 \\ -u_2 & u_1 & 0 \end{bmatrix} \tag{A.3}$$

The most useful property of the skew symmetric matrices composed from a vector is that a matrix form of the cross product vector is made available. Therefore, the matrix product of $S(\vec{u})$ and $\vec{v}$ correspond to the vector cross product of $\vec{u} \wedge \vec{v}$:

$$S(\vec{u})\vec{v} = \begin{bmatrix} 0 & -u_3 & u_2 \\ u_3 & 0 & -u_1 \\ -u_2 & u_1 & 0 \end{bmatrix} \begin{bmatrix} v_1 \\ v_2 \\ v_3 \end{bmatrix} = \begin{bmatrix} u_2v_3 - u_3v_2 \\ u_3v_1 - u_1v_3 \\ u_1v_2 - u_2v_1 \end{bmatrix} = \vec{u} \wedge \vec{v} \tag{A.4}$$

B

Transformations Between Reference Frames

The reference frames that have been used through the thesis are described in section 3.1. In this appendix, the transformation between reference frames will be derived.

A transformation matrix, also called Direction Cosine Matrix (DCM), is a matrix that represents the relative rotation of two different orthogonal frames. Furthermore, given two orthogonal reference frames A

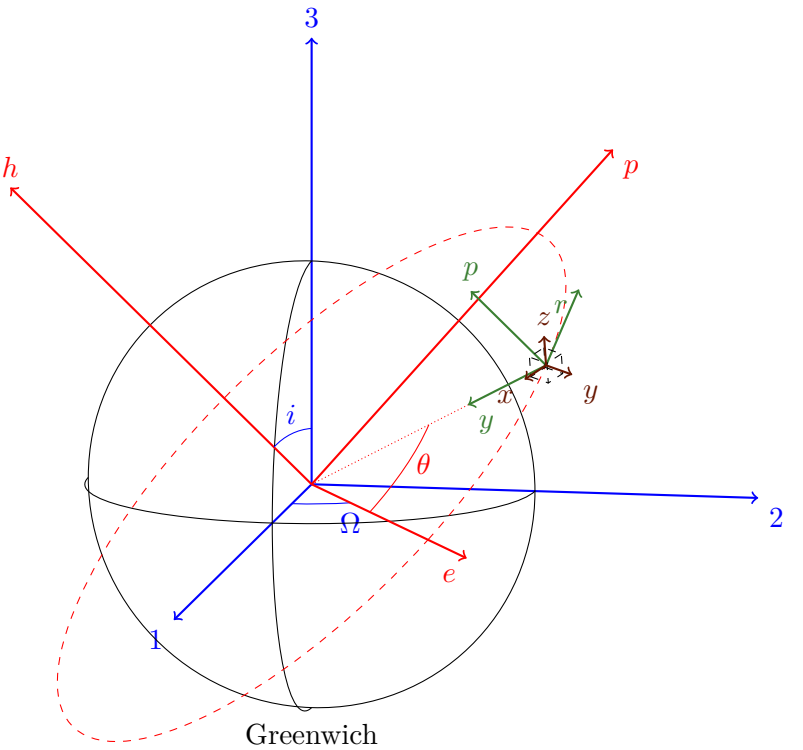

Earth

Earth Centered Earth Fixed (ECEF) Frame

Orbit Perifocal (orb) Frame

Local Vertical Local Horizontal (LVLH) Frame

Principal Inertia (PI) Body Frame

where Ω is the Right Ascension of the Ascending Node (RAAN), i is the orbit inclination and θ is the satellite anomaly.

Figure B.1: Reference Systems

and B, the transformation matrix S_A^B can also be used to calculate the representation of a vector v in frame B (v_B) from the representation in frame A (v_A) (see equation B.1).

$$v_B = S_A^B \cdot v_A \tag{B.1}$$

The transformation matrix can also be transposed to calculate the opposite transformation as in equation B.2.

$$v_A = \left(S_A^B\right)^T \cdot v_B \tag{B.2}$$

For a more broader discussion of the transformation matrix properties, refer to [91].

In this work, DCMs are used to transform vectors between the different reference frames described in figure 3.1. Figure 3.1 is reproduced in figure B.1 for clarification.

B.1 Transformation between ECEF and orb Frame

ECEF and orb Frames are used to represent the satellite position in the calculation of the Earth Magnetic Field in the satellite point. The DCM that transform from ECEF to orb can be derived splitting the full rotation in two successive rotations, as explained in figure B.2.

First a rotation of Ω around axis 3 is performed. The new axis are $1'$, $2'$ and $3 = 3'$. Next, a rotation of angle i around axis $1' = e$ results in the desired orb axis. The transformation is expressed by equation B.3.

$$S_{ECEF}^{orb} = \begin{bmatrix} 1 & 0 & 0 \\ 0 & \cos(i) & \sin(i) \\ 0 & -\sin(i) & \cos(i) \end{bmatrix} \begin{bmatrix} \cos(\Omega) & \sin(\Omega) & 0 \\ -\sin(\Omega) & \cos(\Omega) & 0 \\ 0 & 0 & 1 \end{bmatrix} \tag{B.3}$$

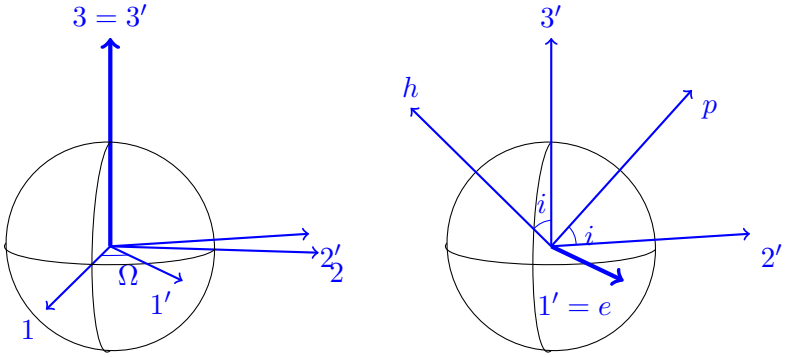

Figure B.2: ECEF to orb transformation

B.2 Transformation between orb and LVLH Frame

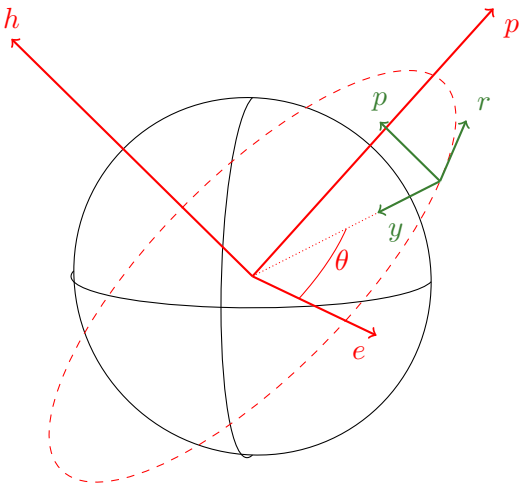

Figure B.3: orb to LVLH transformation

The DCM in the transformation between orb and LVLH frame is represented in figure B.3. Only a rotation of $90 + \theta$ around the h axis

is needed. It is also expressed in equation B.4

$$S_{orb}^{LVLH} = \begin{bmatrix} \cos(90+\theta) & \sin(90+\theta) & 0 \\ -\sin(90+\theta) & \cos(90+\theta) & 0 \\ 0 & 0 & 1 \end{bmatrix} \tag{B.4}$$

In general, a vector transformation between these coordinate frames also requires a translation, because the centers are not the same. However, this transformation is used in this thesis as the first partial rotation to transform the Earth magnetic field vector into the pi frame. And the Earth magnetic field vector can be centered in the center of the LVLH frame. Therefore, the transformation needed does not require the translation.

B.3 Transformation between LVLH and pi frame

The LVLH frame represents the target attitude for the control. Therefore, the rotation of the pi frame with respect to the LVLH frame is the transformation that needs to be taken to 0. The quaternion in the state vector described in section 3.4 are used to represent the *error* between the pi and the LVLH frame. Thus this quaternion is used to represent the rotation between the LVLH and the pi frame given by equation B.5.

$$S_{LVLH}^{pi} = \left[(q_0^2 - q_v^T q_v)I_3 + 2q_v q_v^T - 2q_0 S(q_v)\right] \tag{B.5}$$

C

Introduction To Quaternions

Quaternions were born as an extension in three dimensions of a complex number. They were first developed by Hamilton[92], but the Hamiltonian algebra is written in a general form. When the quaternions are used for attitude representation, a simpler algebra can be derived. This algebra is presented in this appendix.

C.1 Quaternion representation of a rotation

Let $\vec{u}$ be a unit vector and ϕ be an angle. Provided that $\vec{u}$ is the rotation vector and ϕ is the angle of rotation around that vector, the

quaternion is defined by equation C.1.

$$\begin{aligned} q_0 &= \cos\left(\frac{\phi}{2}\right) \\ q_1 &= u_1 \sin\left(\frac{\phi}{2}\right) \\ q_2 &= u_2 \sin\left(\frac{\phi}{2}\right) \\ q_3 &= u_3 \sin\left(\frac{\phi}{2}\right) \end{aligned} \tag{C.1}$$

The quaternion can be represented as $Q = [q_0, q_1, q_2, q_3]$ or equivalently by a scalar and a three dimensional vector $Q = \{q_0, \vec{q}\}$ with $\vec{q} = [q_1, q_2, q_3]$. Both forms are commonly used, as the former expression fits well for matrix implementations while the later is useful for formula derivation and shorthand notation.

C.2 Consecutive rotations

Quaternions can be operated among then in a similar way as vectors or imaginary numbers. However, the most important operation for attitude representation is the multiplication operation. The result of the multiplication of two quaternions has the property to concatenate the rotations represented by the quaternion in another quaternion. The multiplication operation is mathematically described in equation C.2.

$$\begin{aligned} P * Q &= [p_0, p_1, p_2, p_3] * [q_0, q_1, q_2, q_3] \\ &= \begin{bmatrix} p_0q_0 - p_1q_1 - p_2q_2 - p_3q_3 \\ p_1q_0 + p_0q_1 + p_2q_3 - p_3q_2 \\ p_2q_0 + p_0q_2 + p_3q_1 - p_1q_3 \\ p_3q_0 + p_0q_3 + p_1q_2 - p_2q_1 \end{bmatrix} \\ &= (p_0q_0 - \vec{p} \cdot \vec{q}, p_0\vec{q} + q_0\vec{p} + \vec{p} \wedge \vec{q} \end{aligned} \tag{C.2}$$

C.3 Quaternion Rotation matrix

As described before, quaternions can represent a rotation. Sometimes, rotation matrices are more useful than quaternion multiplication, spe-

cially because they can operate over three dimensions regular vectors. The transformation to a Direction Cosine Matrix is represented in equation C.3. The demonstration can be found in reference [91].

$$C = \left(q_0^2 - \vec{q}'\vec{q}\right) I_3 + 2\vec{q}\vec{q}' - 2q_0 S(\vec{q}) \tag{C.3}$$